

Current Status of LIGO-Virgo-KAGRA + Current LVK papers



KAGRA Feb 4

Gravitational Wave Detector Network		
Operational Snapshot as of Feb 04, 13:25 UTC		
Detector	Status	Duration
GEO 600	Unlocked	2:45
LIGO Hanford	Down	>44:15
LIGO Livingston	Down	>44:15
Virgo	Info too old	
KAGRA	Down	>44:16

[Detector status summary pages](#)
[LVK links](#)

[gwistat](#)

LIGO Hanford NOHOFT Duration: 2d 16:28:59 (prev: unknown) Last updated at 22:26	LIGO Livingston NOHOFT Duration: 7d 08:46:59 (prev: unknown) Last updated at 22:26	Virgo UNKNOWN Duration: 21d 07:48:53 (prev: nohoft) Last updated at 2:49	KAGRA UNKNOWN Duration: 101d 08:10:59 (prev: nohoft) Last updated at 22:26	Thu Feb 04 2021 22:26:38 1296480416
DMT Call John Zweizig 2 / 15 CRITICAL Last updated at 22:26	Low-latency Data 1 / 45 WARNING 3 / 45 UNKNOWN Last updated at 22:26	LIGO Data Replicator 2 / 14 WARNING Last updated at 22:26	DetChar Summary 1 / 22 UNKNOWN Last updated at 22:26	DetChar Jobs 1 / 16 UNKNOWN Last updated at 22:26
GraceDB 1 OK Last updated at 22:26	LVAAlert 2 OK Last updated at 22:26	GraceDB Playground 1 OK Last updated at 22:26	DQSegDB 15 OK Last updated at 22:26	NDS 28 OK Last updated at 22:26
gstLAL Inspiral 3 OK Last updated at 22:26	CIS 2 OK Last updated at 22:26	EMFollow 2 OK Last updated at 22:26	PyCBC Live 1 OK Last updated at 22:26	Auth 27 OK Last updated at 22:26

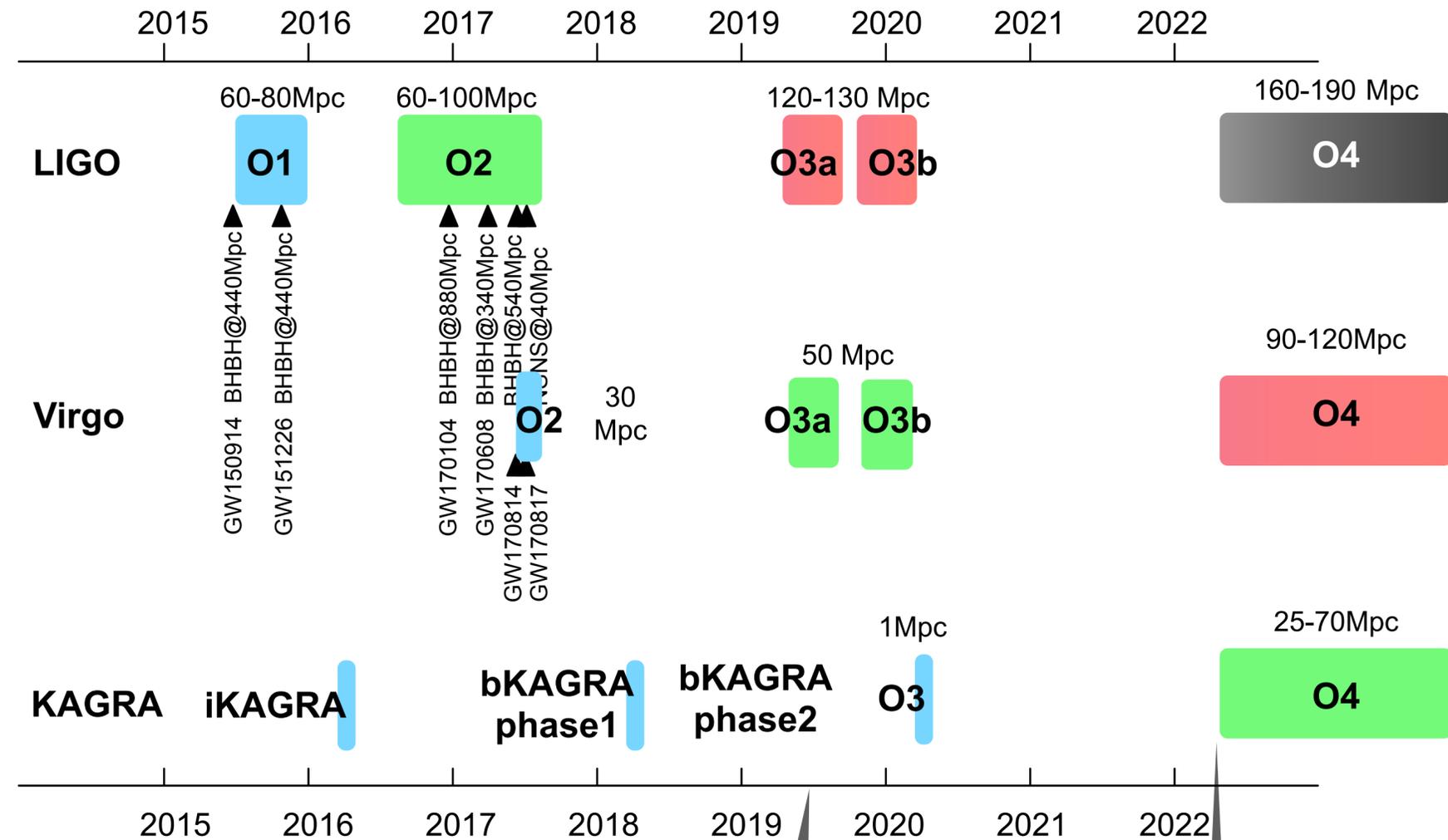
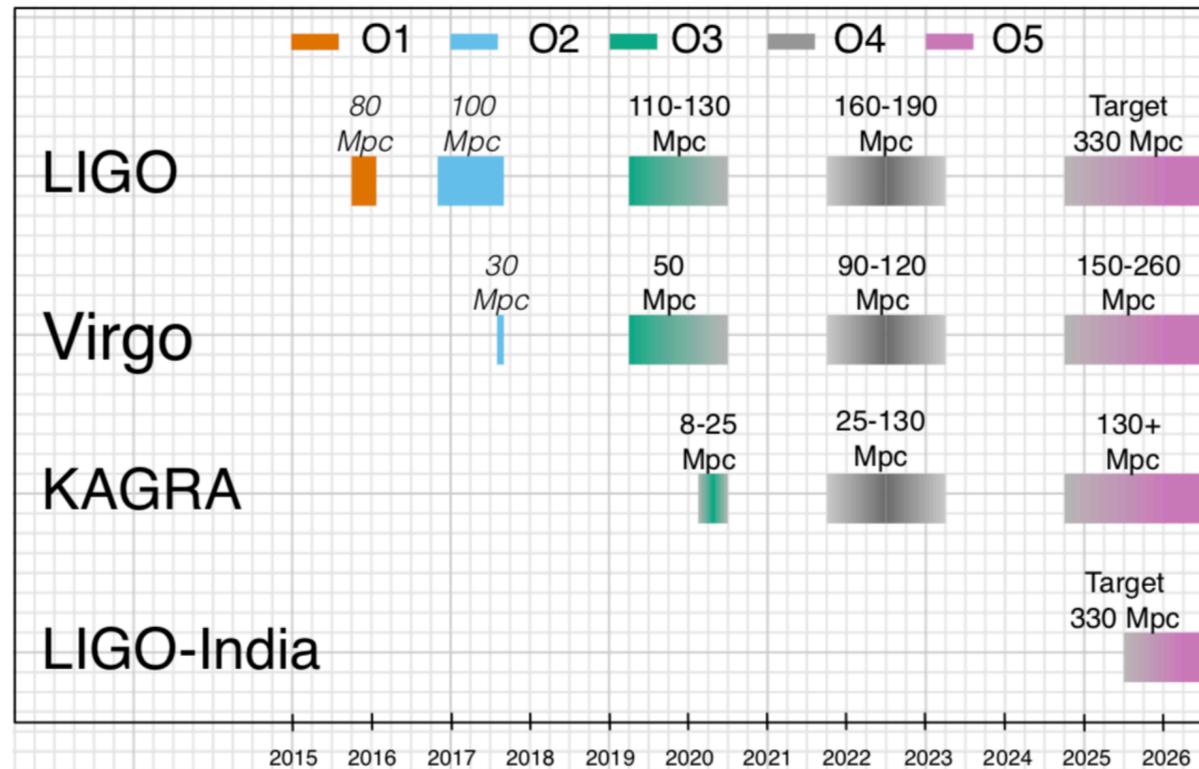
<https://monitor.ligo.org/gwstatus>

真貝寿明 Hisaaki Shinkai
 大阪工業大学情報科学部

<http://www.oit.ac.jp/is/shinkai/>



Target Sensitivity & Schedule



“Scenario Paper” [1304.0670ver2020Jan]

LVK collaboration, Living Rev Relativ (2020) 23:3

<https://link.springer.com/article/10.1007/s41114-020-00026-9>

- O1 (2015/9/12 - 2016/1/19) LIGO
- O2 (2016/11/30 - 2017/8/25) LIGO+Virgo
- O3a (2019/4/1 - 2019/9/30) LIGO+Virgo
- O3b (2019/10/1 - 2020/3/27) LIGO+Virgo + KAGRA

Oct 2019, KAGRA joined LV network

COVID-19 terminated O3b

O4 will likely start no earlier than June 2022

銀河系スケール から 銀河群スケールへ

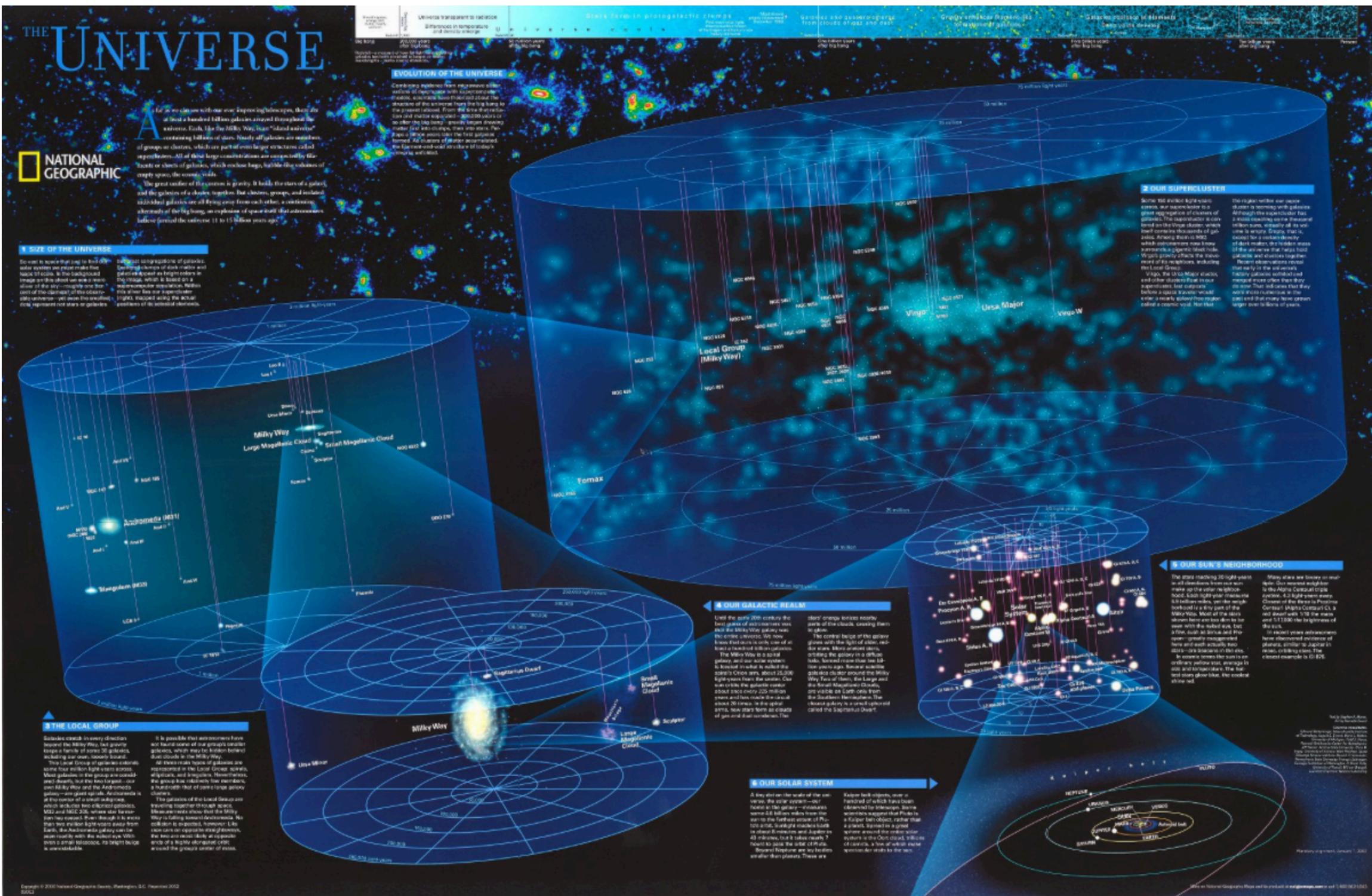
1 pc = 3.26光年
(年周視差1秒角となる距離)

天の川銀河 直径 10万光年
32.5 kpc

大マゼラン雲 (LMC) 50 kpc
小マゼラン雲 (SMC) 61 kpc

アンドロメダ銀河 (M31)
0.79 Mpc = 250万光年

おとめ座銀河団 (Virgo Cluster)
16.5 Mpc = 5380万光年



National Geographic Universe Reference Map

銀河団スケール から 大規模構造 へ

おとめ座銀河団(Virgo Cluster)
16.5 Mpc=5380万光年

CfA2 Great Wall
110-160 Mpc
= 3.5-5.5 億光年

Sloan Great Wall
300 Mpc = 10 億光年

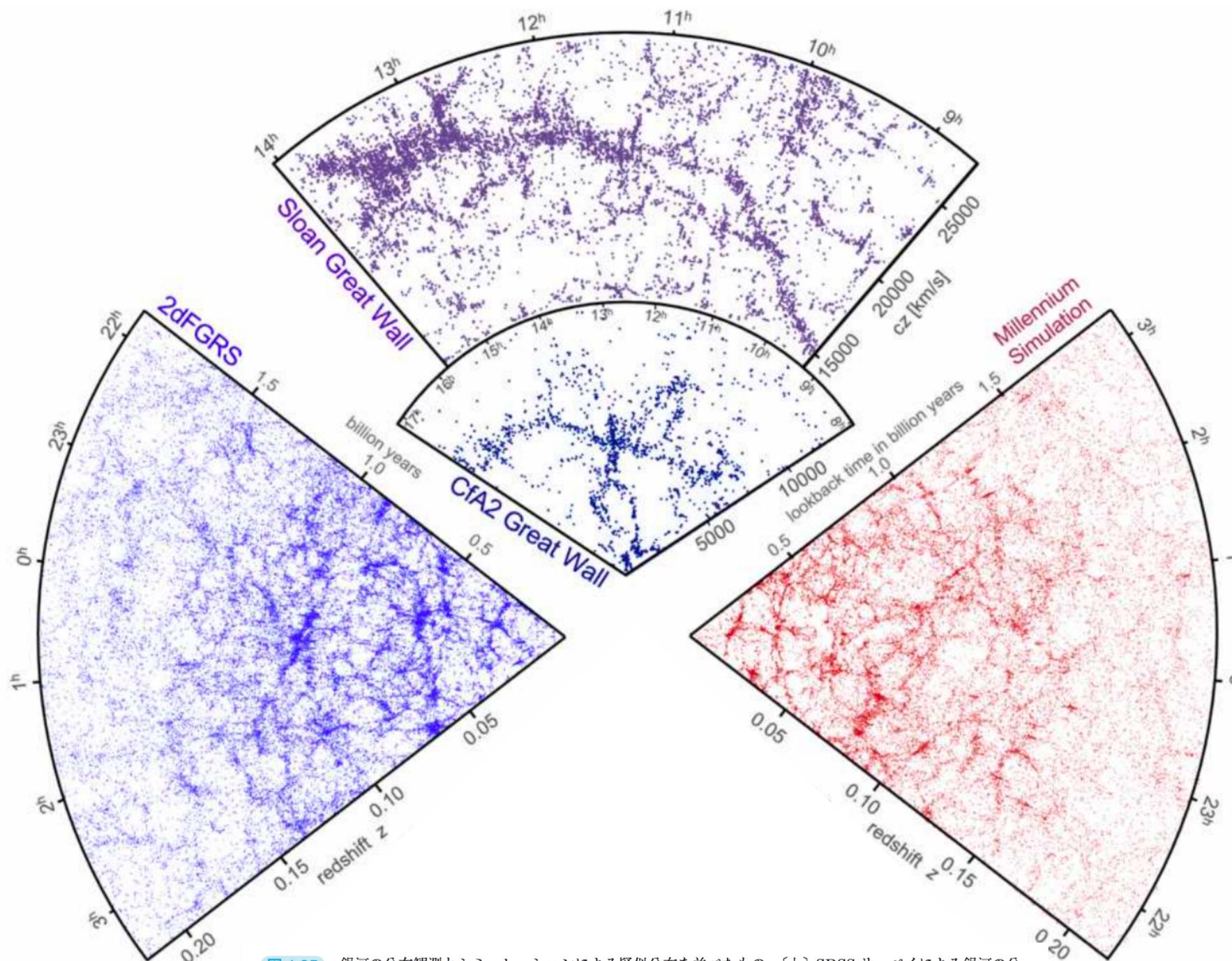
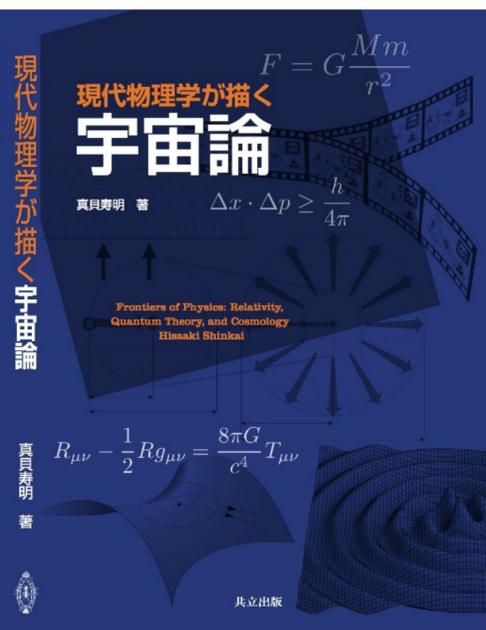
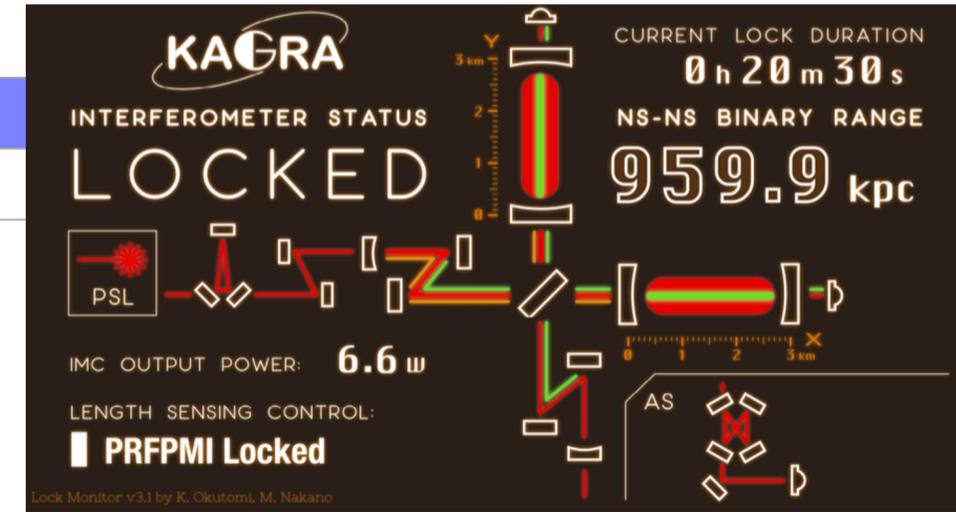
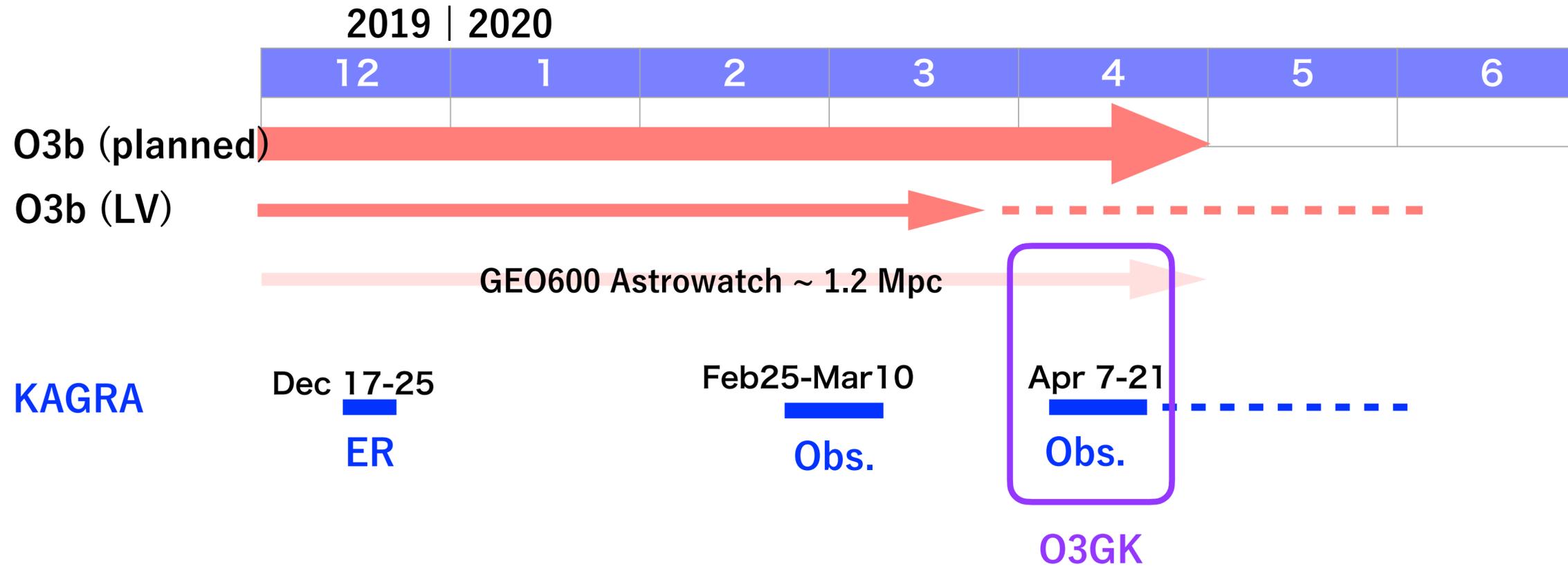


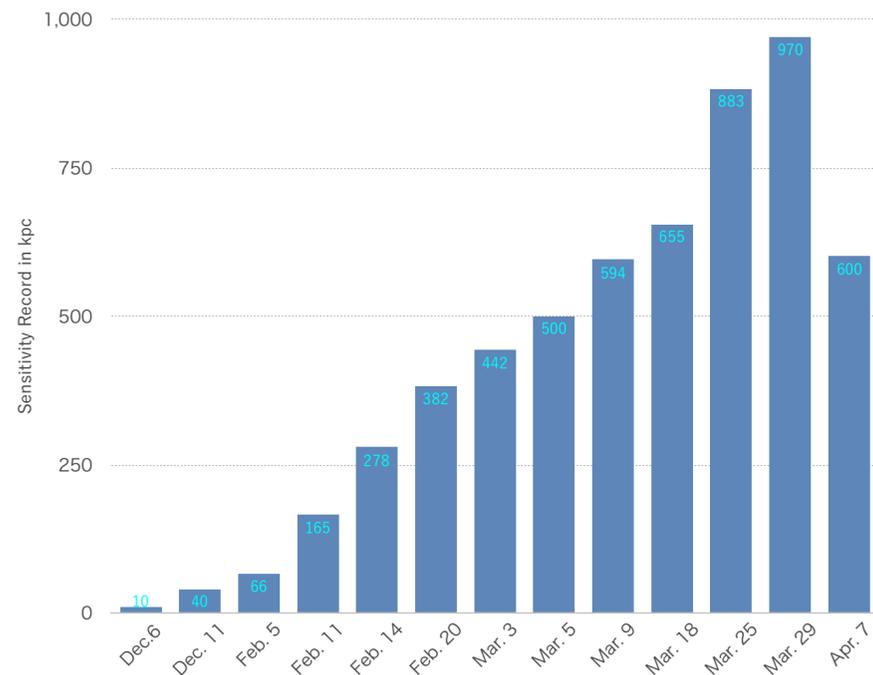
図 1.35 銀河の分布観測とシミュレーションによる疑似分布を並べたもの。[上] SDSS サーベイによる銀河の分布図と図 1.34 を重ねたもの。SDSS は、北天から見える 65 万個以上の銀河を 2 億光年まで示している。1.3 億光年の距離に及ぶ 1 万個以上のグレートウォール (万里の長城) も新たに発見された。[左] 2dFGR サーベイによる銀河の分布図。南天の 22 万個以上の銀河を 2 億光年まで示している。[右] ミレニアム・シミュレーションという数値計算結果を似せて示したもの。[Springel, Frenk, White の論文 (2006) を加工]



O3b, O3GK, and after that

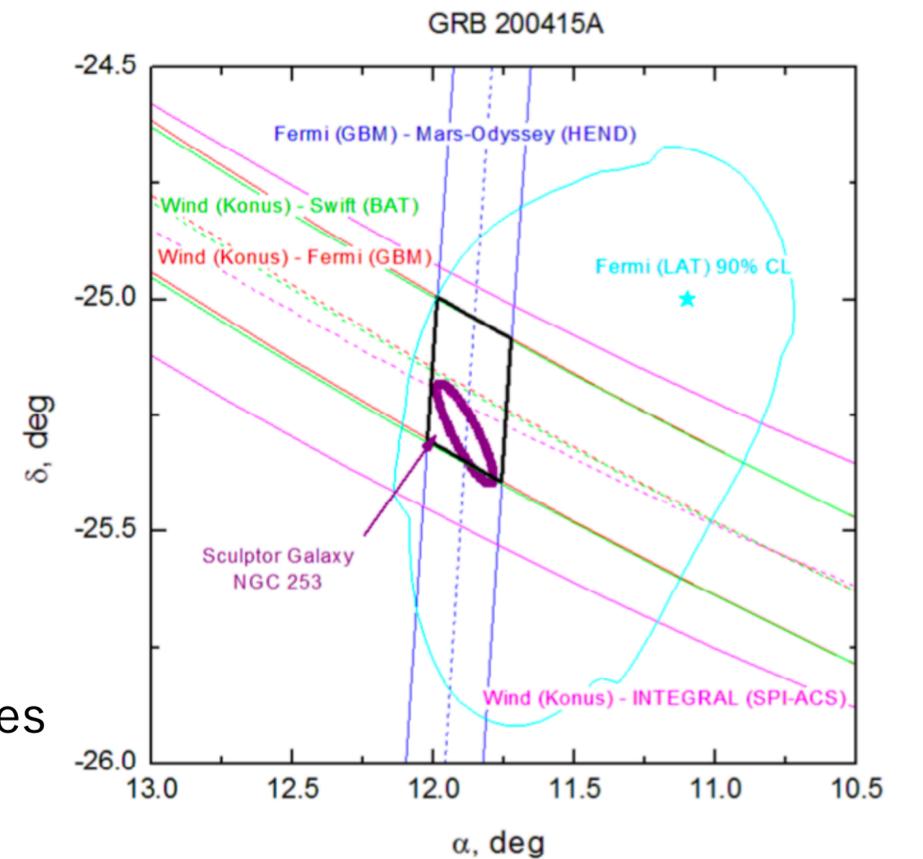


March 29, 2020

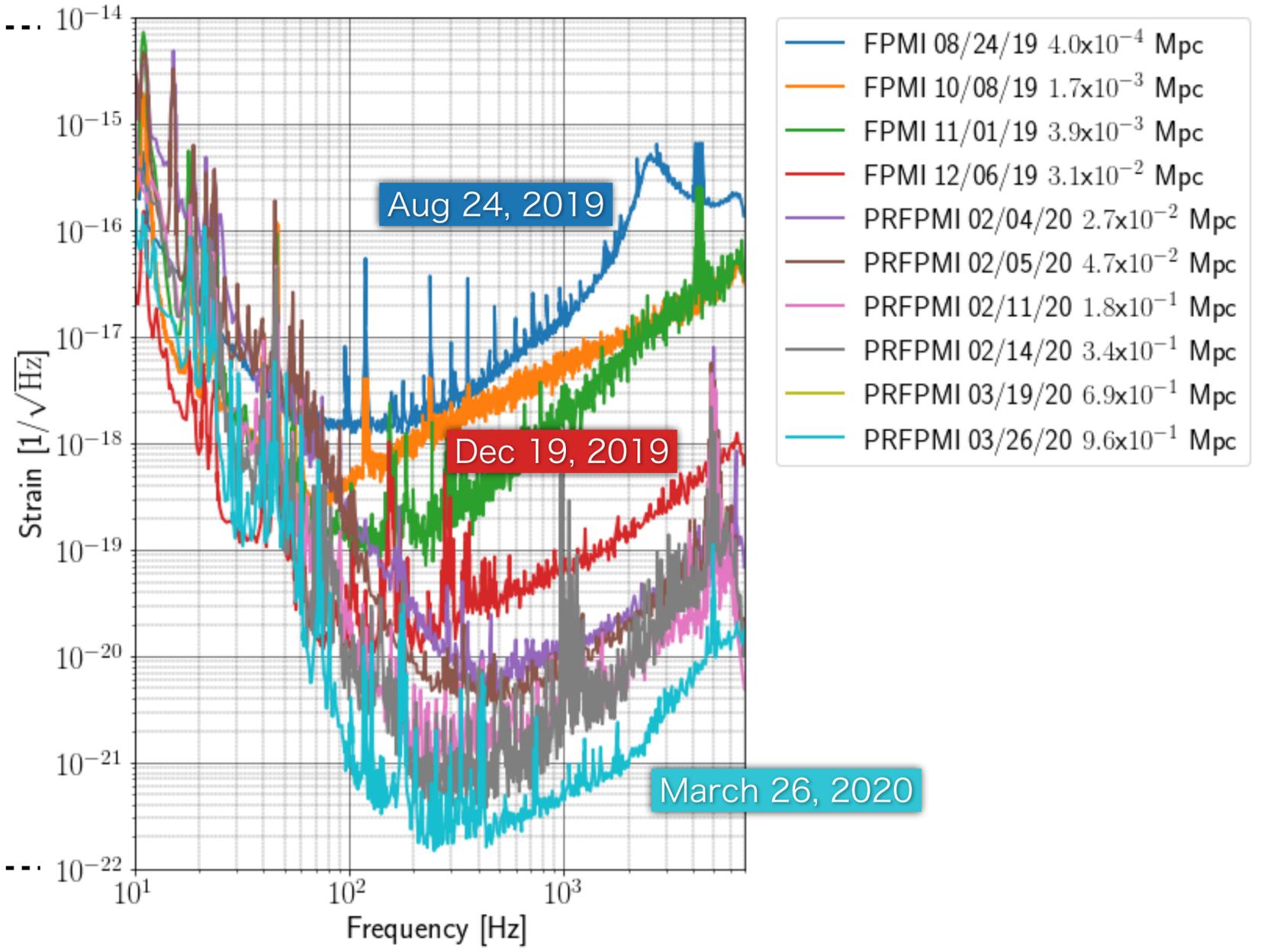
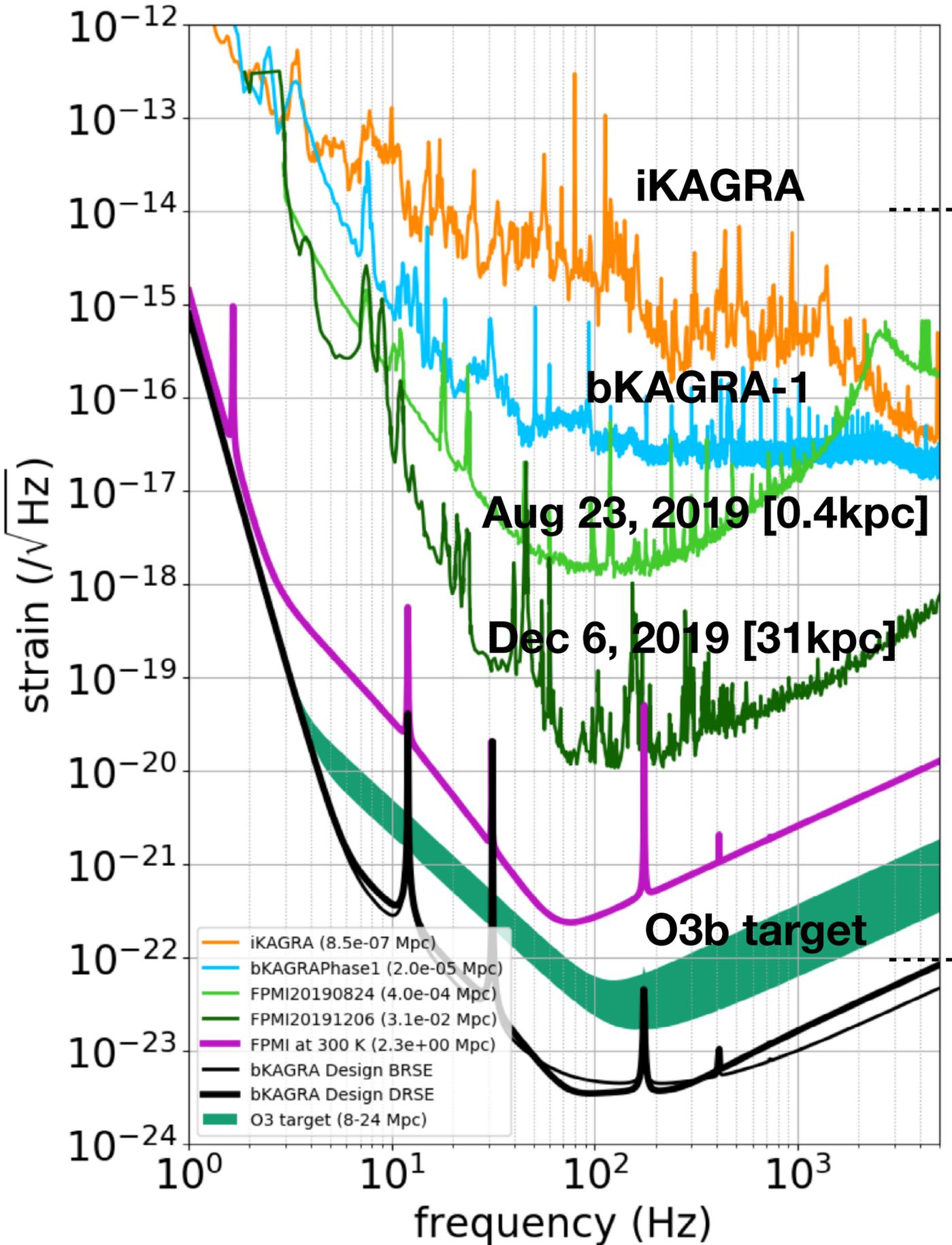


* O3GK observation paper plan (LVK paper)

NGC 235 (Sculptor galaxy)
3.5 Mpc, one of the brightest galaxies
https://gcn.gsfc.nasa.gov/fermi_grbs.html

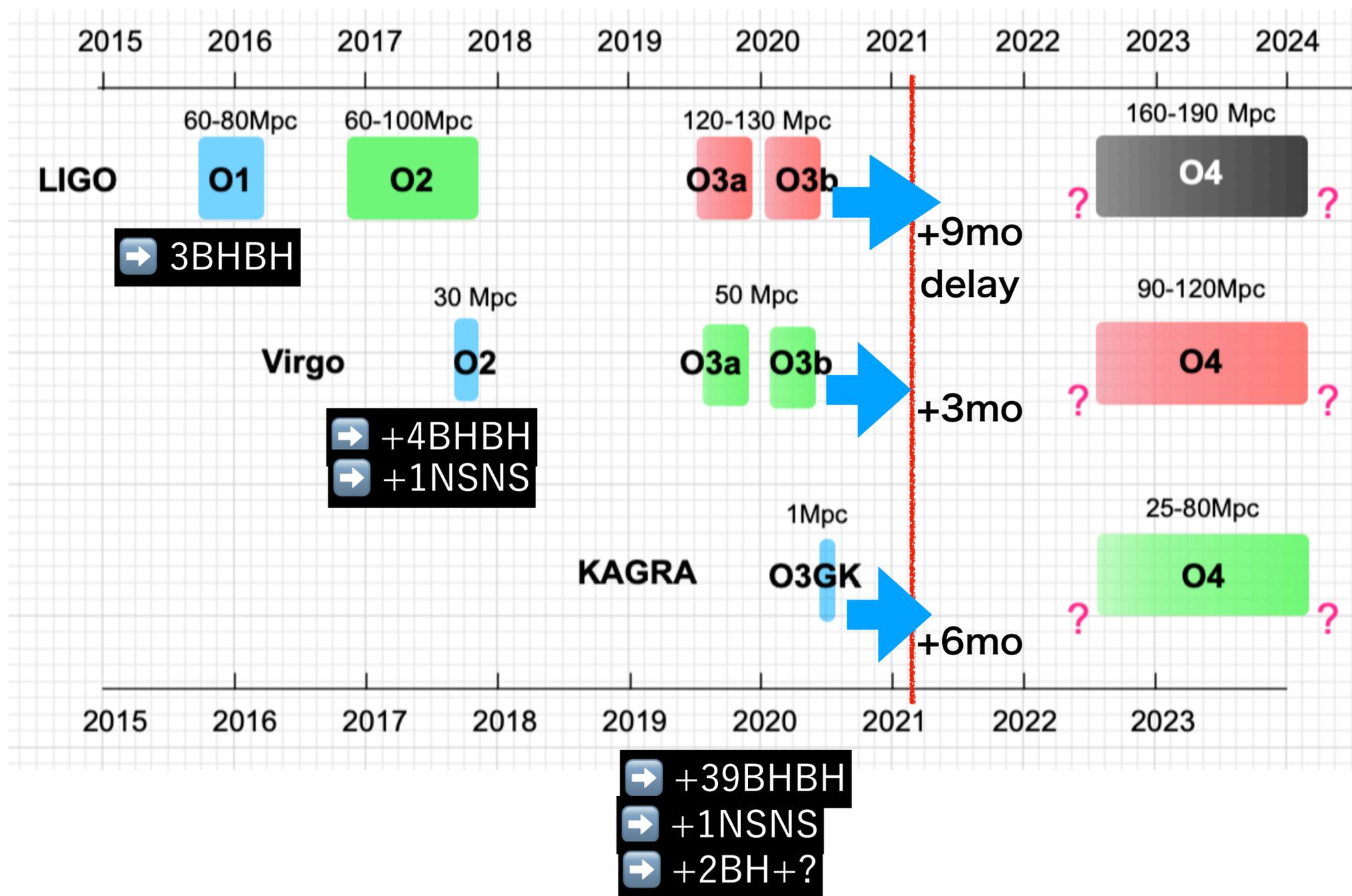


▼ KAGRA actual



What's in 2021?

Five years ago, GW physics was a “future story”. People did not know the existence of BBH, BH over 10 solar mass (except SMBH). Now LIGO/Virgo announced 50 events in October 2020 as GWTC-2 up to their O3a.

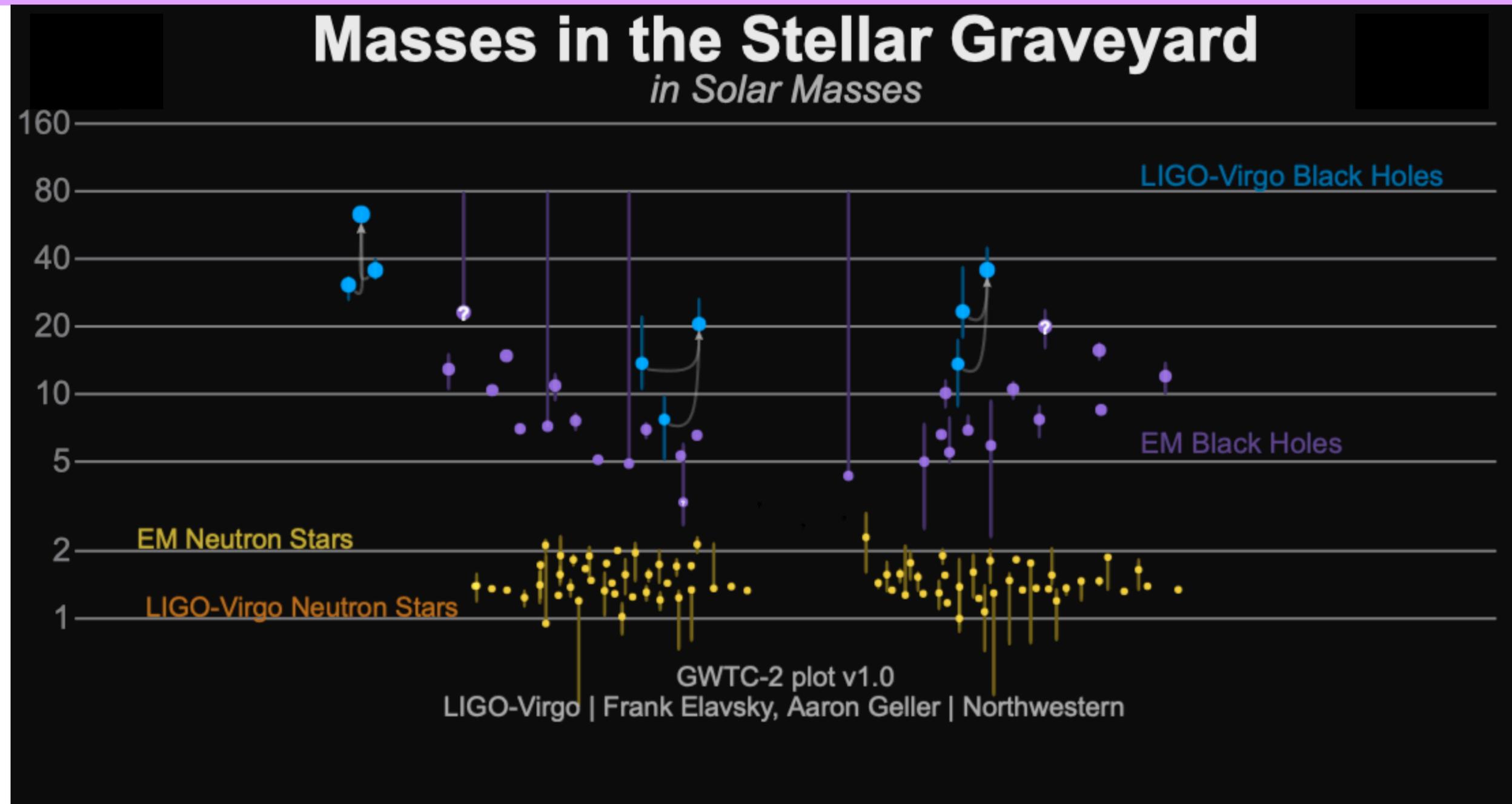


2021 Spring : O3a final analysis
 : O3a data release
 : O3b catalog
 2021 Fall : O3b final analysis
 : O3b data release

2021
 LIGO Hanford: Upgrade
 LIGO Livingston: Upgrade
 Virgo : Upgrade -> Test Run
 KAGRA : Upgrade

2022 June or later
 LVK O4 start

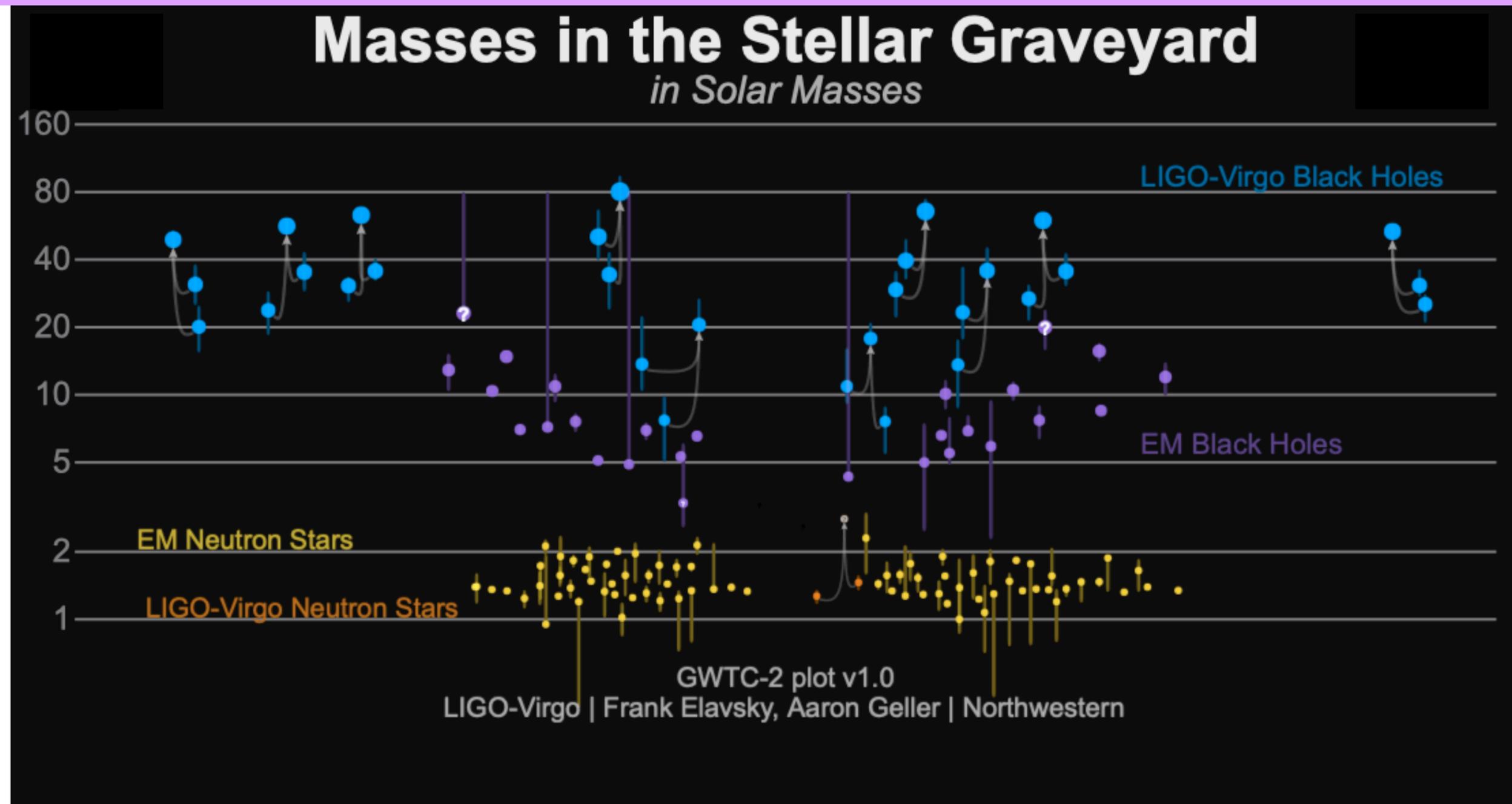
O1 (2015/9/12 - 2016/1/19)



3 BHBH

GW150914: the first ever detection of gravitational waves from the merger of two black holes more than a billion light years away

<https://media.ligo.northwestern.edu/gallery/mass-plot>

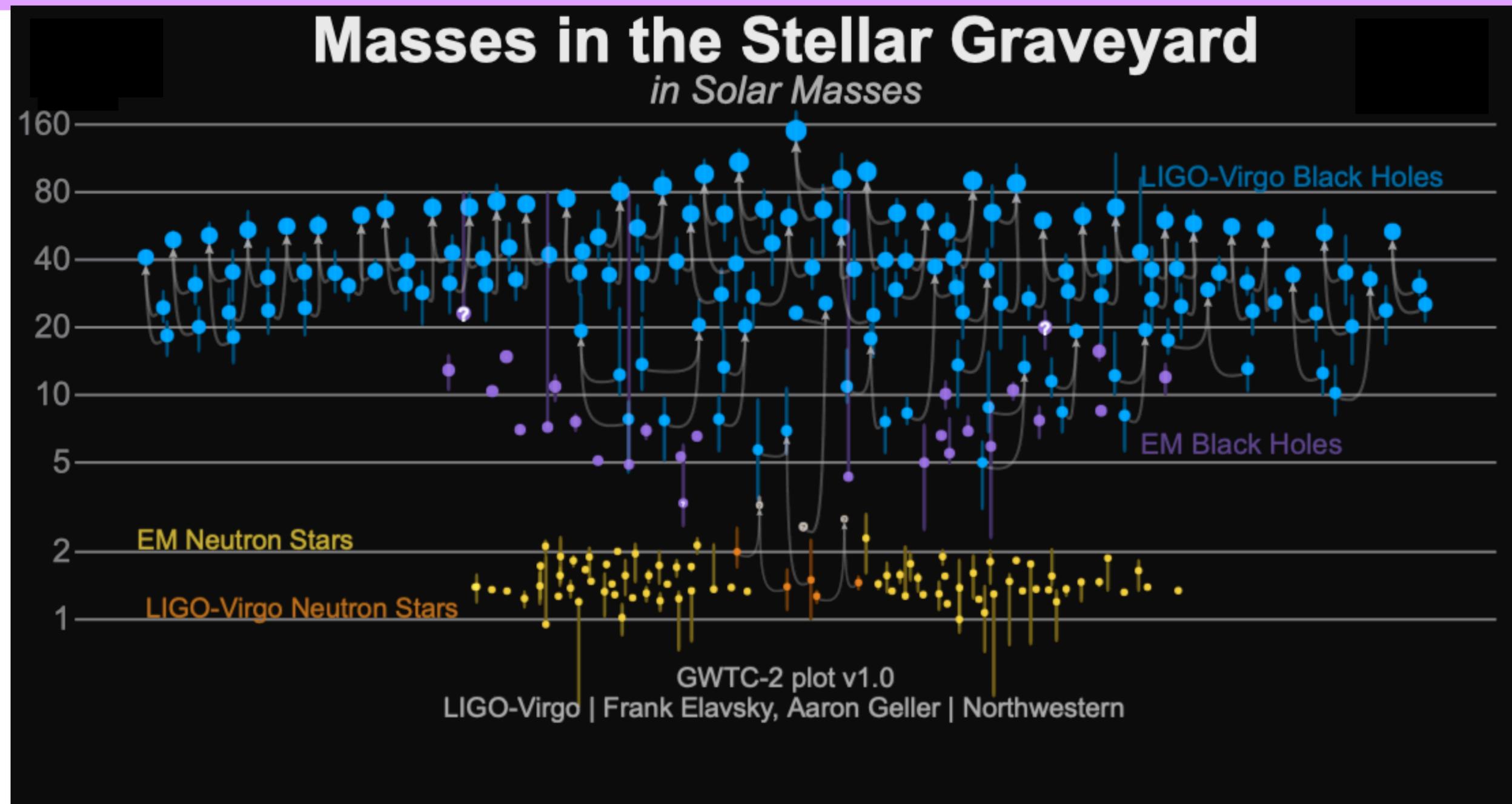


- **GW170814**: the first GW signal measured by the three-detector network, also from a binary black hole (BBH) merger;
- **GW170817**: the first GW signal measured from a binary neutron star (BNS) merger — and also the first event observed in light, by dozens of telescopes across the entire electromagnetic spectrum.

<https://media.ligo.northwestern.edu/gallery/mass-plot>

O3a (2019/4/1 - 2019/9/30)

After O3a : GWTC2 (2020/10/28 released)



46 BHBH
2 NSNS
2 BH+?

- [GW190412](#): the first BBH with definitively asymmetric component masses, which also shows evidence for [higher harmonics](#)
- [GW190425](#): the second gravitational-wave event consistent with a BNS, following [GW170817](#)
- [GW190426_152155](#): a low-mass event consistent with either an NSBH or BBH
- [GW190514_065416](#): a BBH with the smallest effective aligned spin of all O3a events
- [GW190517_055101](#): a BBH with the largest effective aligned spin of all O3a events
- [GW190521](#): a BBH with total mass over 150 times the mass of the Sun
- [GW190814](#): a highly asymmetric system of ambiguous nature, corresponding to the merger of a 23 solar mass black hole with a 2.6 solar mass compact object, making the latter either the lightest black hole or heaviest neutron star observed in a compact binary
- [GW190924_021846](#): likely the lowest-mass BBH, with both black holes exceeding 3 solar masses

2. 重力波観測の現状

GWTC-2 (突発的重力波カタログ2)

Gravitational Wave Transient Catalog 2

[arXiv:2010.14527](https://arxiv.org/abs/2010.14527)

<https://dcc.ligo.org/LIGO-P2000223/public>

39 events in O3a

36BHBH, 1 NSNS, 2 BH+unknown

GWyymmdd_hhmmss for new events

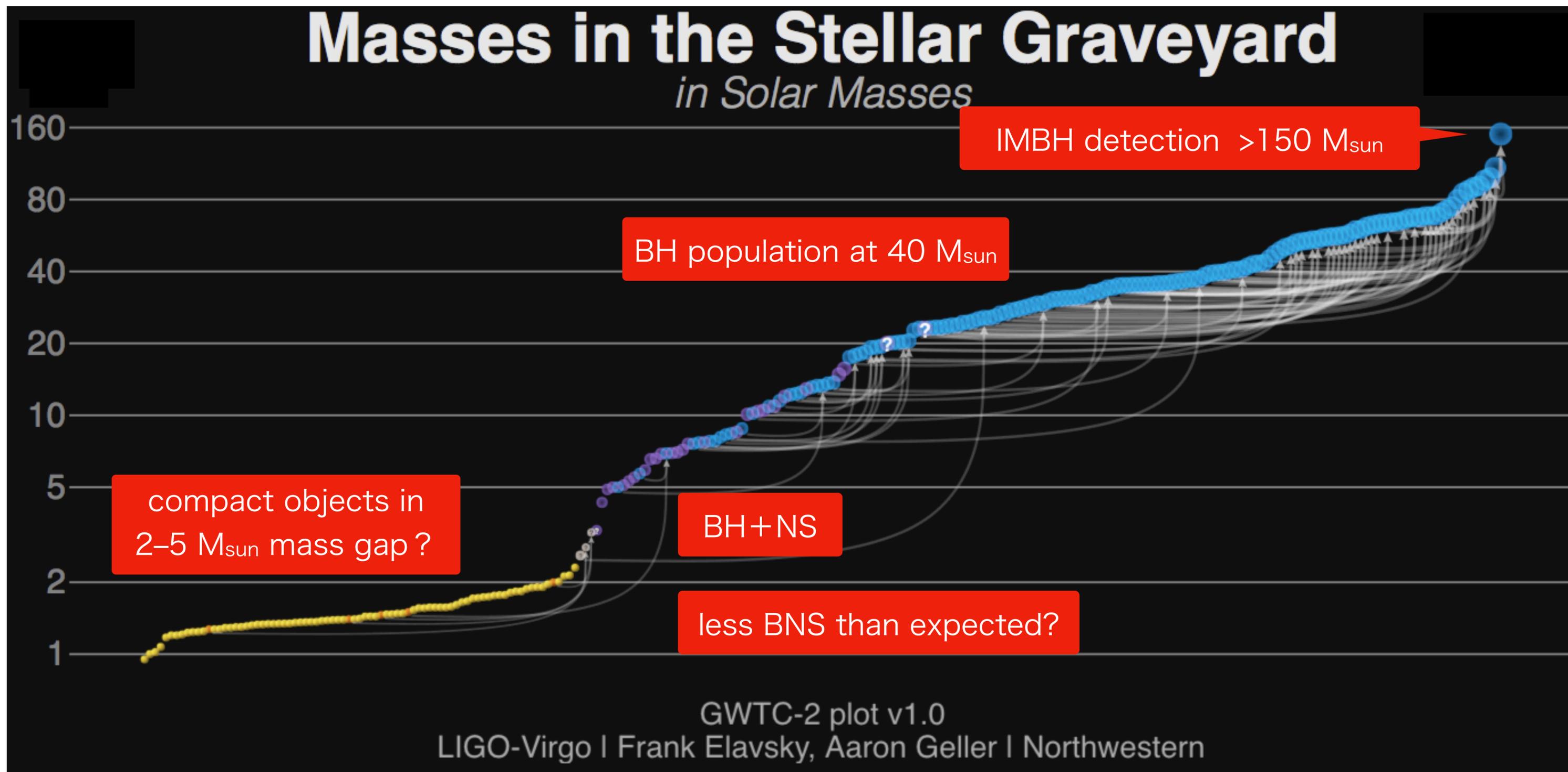
False-Alarm Rate < 2/1yr

- **GW190412**: the first BBH with definitively asymmetric component masses, which also shows evidence for **higher harmonics**
- **GW190425**: the second gravitational-wave event consistent with a BNS, following **GW170817**
- **GW190426_152155**: a low-mass event consistent with either an NSBH or BBH
- **GW190514_065416**: a BBH with the smallest effective aligned spin of all O3a events
- **GW190517_055101**: a BBH with the largest effective aligned spin of all O3a events
- **GW190521**: a BBH with total mass over 150 times the mass of the Sun
- **GW190814**: a highly asymmetric system of ambiguous nature, corresponding to the merger of a 23 solar mass black hole with a 2.6 solar mass compact object, making the latter either the lightest black hole or heaviest neutron star observed in a compact binary
- **GW190924_021846**: likely the lowest-mass BBH, with both black holes exceeding 3 solar masses

[arXiv:2010.14529](https://arxiv.org/abs/2010.14529) Test of GR

[arXiv:2010.14533](https://arxiv.org/abs/2010.14533) Population properties

Event	M (M_{\odot})	M (M_{\odot})	m_1 (M_{\odot})	m_2 (M_{\odot})	χ_{eff}	D_L (Gpc)	z	M_f (M_{\odot})	χ_f	$\Delta\Omega$ (deg ²)	SNR
GW190408_181802	42.9 ^{+4.1} _{-2.9}	18.3 ^{+1.8} _{-1.2}	24.5 ^{+5.1} _{-3.4}	18.3 ^{+3.2} _{-3.5}	-0.03 ^{+0.13} _{-0.19}	1.58 ^{+0.40} _{-0.59}	0.30 ^{+0.06} _{-0.10}	41.0 ^{+3.8} _{-2.7}	0.67 ^{+0.06} _{-0.07}	140	15.3 ^{+0.2} _{-0.3}
GW190412	38.4 ^{+3.8} _{-3.7}	13.3 ^{+0.4} _{-0.3}	30.0 ^{+4.7} _{-5.1}	8.3 ^{+1.6} _{-0.9}	0.25 ^{+0.08} _{-0.11}	0.74 ^{+0.14} _{-0.17}	0.15 ^{+0.03} _{-0.03}	37.3 ^{+3.9} _{-3.9}	0.67 ^{+0.05} _{-0.06}	21	18.9 ^{+0.2} _{-0.3}
GW190413_052954	56.9 ^{+13.1} _{-8.9}	24.0 ^{+5.4} _{-3.7}	33.4 ^{+12.4} _{-7.4}	23.4 ^{+6.7} _{-6.3}	0.01 ^{+0.29} _{-0.33}	4.10 ^{+2.41} _{-1.89}	0.66 ^{+0.30} _{-0.27}	54.3 ^{+12.4} _{-8.4}	0.69 ^{+0.12} _{-0.13}	1400	8.9 ^{+0.4} _{-0.8}
GW190413_134308	76.1 ^{+15.9} _{-10.6}	31.9 ^{+7.3} _{-4.6}	45.4 ^{+13.6} _{-9.6}	30.9 ^{+10.2} _{-9.6}	-0.01 ^{+0.24} _{-0.28}	5.15 ^{+2.44} _{-2.34}	0.80 ^{+0.30} _{-0.31}	72.8 ^{+15.2} _{-10.3}	0.69 ^{+0.10} _{-0.12}	520	10.0 ^{+0.4} _{-0.5}
GW190421_213856	71.8 ^{+12.5} _{-8.6}	30.7 ^{+5.5} _{-3.9}	40.6 ^{+10.4} _{-6.6}	31.4 ^{+7.5} _{-8.2}	-0.05 ^{+0.23} _{-0.26}	3.15 ^{+1.37} _{-1.42}	0.53 ^{+0.18} _{-0.21}	68.6 ^{+11.7} _{-8.1}	0.68 ^{+0.10} _{-0.11}	1000	10.7 ^{+0.2} _{-0.4}
GW190424_180648	70.7 ^{+13.4} _{-9.8}	30.3 ^{+5.7} _{-4.2}	39.5 ^{+10.9} _{-6.9}	31.0 ^{+7.4} _{-7.3}	0.15 ^{+0.22} _{-0.22}	2.55 ^{+1.56} _{-1.33}	0.45 ^{+0.22} _{-0.21}	67.1 ^{+12.5} _{-9.2}	0.75 ^{+0.08} _{-0.09}	26000	10.4 ^{+0.2} _{-0.4}
GW190425	3.4 ^{+0.3} _{-0.1}	1.44 ^{+0.02} _{-0.02}	2.0 ^{+0.6} _{-0.3}	1.4 ^{+0.3} _{-0.3}	0.06 ^{+0.11} _{-0.05}	0.16 ^{+0.07} _{-0.07}	0.03 ^{+0.01} _{-0.02}	—	—	9900	12.4 ^{+0.3} _{-0.4}
GW190426_152155	7.2 ^{+3.5} _{-1.5}	2.41 ^{+0.08} _{-0.08}	5.7 ^{+4.0} _{-2.3}	1.5 ^{+0.8} _{-0.5}	-0.03 ^{+0.33} _{-0.30}	0.38 ^{+0.19} _{-0.16}	0.08 ^{+0.04} _{-0.03}	—	—	1400	8.7 ^{+0.5} _{-0.6}
GW190503_185404	71.3 ^{+9.3} _{-8.0}	30.1 ^{+4.2} _{-4.0}	42.9 ^{+9.2} _{-7.8}	28.5 ^{+7.5} _{-7.9}	-0.02 ^{+0.20} _{-0.26}	1.52 ^{+0.71} _{-0.66}	0.29 ^{+0.11} _{-0.11}	68.2 ^{+8.7} _{-7.5}	0.67 ^{+0.09} _{-0.12}	94	12.4 ^{+0.2} _{-0.3}
GW190512_180714	35.6 ^{+3.9} _{-3.4}	14.5 ^{+1.3} _{-1.0}	23.0 ^{+5.4} _{-5.7}	12.5 ^{+3.5} _{-2.5}	0.03 ^{+0.13} _{-0.13}	1.49 ^{+0.53} _{-0.59}	0.28 ^{+0.09} _{-0.10}	34.2 ^{+3.9} _{-3.4}	0.65 ^{+0.07} _{-0.07}	230	12.2 ^{+0.2} _{-0.4}
GW190513_205428	53.6 ^{+8.6} _{-5.9}	21.5 ^{+3.6} _{-1.9}	35.3 ^{+9.6} _{-9.0}	18.1 ^{+7.3} _{-4.2}	0.12 ^{+0.29} _{-0.18}	2.16 ^{+0.94} _{-0.80}	0.39 ^{+0.14} _{-0.13}	51.3 ^{+8.1} _{-5.8}	0.69 ^{+0.14} _{-0.12}	490	12.9 ^{+0.3} _{-0.4}
GW190514_065416	64.2 ^{+16.6} _{-9.6}	27.4 ^{+6.9} _{-4.3}	36.9 ^{+13.4} _{-7.3}	27.5 ^{+8.2} _{-7.7}	-0.16 ^{+0.28} _{-0.32}	4.93 ^{+2.76} _{-2.41}	0.77 ^{+0.34} _{-0.33}	61.6 ^{+16.0} _{-9.2}	0.64 ^{+0.11} _{-0.14}	2400	8.2 ^{+0.3} _{-0.6}
GW190517_055101	61.9 ^{+10.0} _{-9.6}	26.0 ^{+4.2} _{-4.0}	36.4 ^{+11.8} _{-7.8}	24.8 ^{+6.9} _{-7.1}	0.53 ^{+0.20} _{-0.19}	2.11 ^{+1.79} _{-1.00}	0.38 ^{+0.26} _{-0.16}	57.8 ^{+9.4} _{-9.1}	0.87 ^{+0.05} _{-0.07}	460	10.7 ^{+0.4} _{-0.6}
GW190519_153544	104.2 ^{+14.5} _{-14.9}	43.5 ^{+6.8} _{-6.8}	64.5 ^{+11.3} _{-13.2}	39.9 ^{+11.0} _{-10.6}	0.33 ^{+0.19} _{-0.22}	2.85 ^{+2.02} _{-1.14}	0.49 ^{+0.27} _{-0.17}	98.7 ^{+13.5} _{-14.2}	0.80 ^{+0.07} _{-0.12}	770	15.6 ^{+0.2} _{-0.3}
GW190521	157.9 ^{+37.4} _{-20.9}	66.9 ^{+15.5} _{-9.2}	91.4 ^{+29.3} _{-17.5}	66.8 ^{+20.7} _{-20.7}	0.06 ^{+0.31} _{-0.37}	4.53 ^{+2.30} _{-2.13}	0.72 ^{+0.29} _{-0.29}	150.3 ^{+35.8} _{-20.0}	0.73 ^{+0.11} _{-0.14}	940	14.2 ^{+0.3} _{-0.3}
GW190521_074359	74.4 ^{+6.8} _{-4.6}	31.9 ^{+3.1} _{-2.4}	42.1 ^{+5.9} _{-4.9}	32.7 ^{+5.4} _{-6.2}	0.09 ^{+0.10} _{-0.13}	1.28 ^{+0.38} _{-0.57}	0.25 ^{+0.06} _{-0.10}	70.7 ^{+6.4} _{-4.2}	0.72 ^{+0.05} _{-0.07}	500	25.8 ^{+0.1} _{-0.2}
GW190527_092055	58.5 ^{+27.9} _{-10.6}	24.2 ^{+11.9} _{-4.4}	36.2 ^{+19.1} _{-9.5}	22.8 ^{+12.7} _{-8.1}	0.13 ^{+0.29} _{-0.28}	3.10 ^{+4.85} _{-1.64}	0.53 ^{+0.61} _{-0.25}	55.9 ^{+26.4} _{-10.1}	0.73 ^{+0.12} _{-0.16}	3800	8.1 ^{+0.4} _{-1.0}
GW190602_175927	114.1 ^{+18.5} _{-15.7}	48.3 ^{+8.6} _{-8.0}	67.2 ^{+16.0} _{-12.6}	47.4 ^{+13.4} _{-16.6}	0.10 ^{+0.25} _{-0.25}	2.99 ^{+2.02} _{-1.26}	0.51 ^{+0.27} _{-0.19}	108.8 ^{+17.2} _{-14.8}	0.71 ^{+0.10} _{-0.13}	720	12.8 ^{+0.2} _{-0.3}
GW190620_030421	90.1 ^{+17.3} _{-12.1}	37.5 ^{+7.8} _{-5.7}	55.4 ^{+15.8} _{-12.0}	35.0 ^{+11.6} _{-11.4}	0.34 ^{+0.21} _{-0.25}	3.16 ^{+1.67} _{-1.43}	0.54 ^{+0.22} _{-0.21}	85.4 ^{+15.9} _{-11.4}	0.80 ^{+0.08} _{-0.14}	6700	12.1 ^{+0.3} _{-0.4}
GW190630_185205	58.8 ^{+4.7} _{-4.8}	24.8 ^{+2.1} _{-2.0}	35.0 ^{+6.9} _{-5.7}	23.6 ^{+5.2} _{-5.1}	0.10 ^{+0.12} _{-0.13}	0.93 ^{+0.56} _{-0.50}	0.19 ^{+0.10} _{-0.07}	56.1 ^{+4.5} _{-4.6}	0.70 ^{+0.06} _{-0.07}	1300	15.6 ^{+0.2} _{-0.3}
GW190701_203306	94.1 ^{+11.6} _{-9.3}	40.2 ^{+5.2} _{-4.7}	53.6 ^{+11.7} _{-7.8}	40.8 ^{+8.3} _{-11.5}	-0.06 ^{+0.23} _{-0.28}	2.14 ^{+0.79} _{-0.73}	0.38 ^{+0.12} _{-0.12}	90.0 ^{+10.8} _{-8.6}	0.67 ^{+0.09} _{-0.12}	45	11.3 ^{+0.2} _{-0.4}
GW190706_222641	101.6 ^{+17.9} _{-13.5}	42.0 ^{+8.4} _{-6.2}	64.0 ^{+15.2} _{-15.2}	38.5 ^{+12.5} _{-12.4}	0.32 ^{+0.25} _{-0.30}	5.07 ^{+2.57} _{-2.11}	0.79 ^{+0.31} _{-0.28}	96.3 ^{+16.7} _{-13.2}	0.80 ^{+0.08} _{-0.17}	610	12.6 ^{+0.2} _{-0.4}
GW190707_093326	20.0 ^{+1.9} _{-1.3}	8.5 ^{+0.6} _{-0.4}	11.5 ^{+3.3} _{-1.7}	8.4 ^{+1.4} _{-1.6}	-0.05 ^{+0.10} _{-0.08}	0.80 ^{+0.37} _{-0.38}	0.16 ^{+0.07} _{-0.07}	19.2 ^{+1.9} _{-1.3}	0.66 ^{+0.03} _{-0.04}	1300	13.3 ^{+0.2} _{-0.4}
GW190708_232457	30.8 ^{+2.5} _{-1.8}	13.1 ^{+0.9} _{-0.6}	17.5 ^{+4.7} _{-2.3}	13.1 ^{+2.7} _{-2.7}	0.02 ^{+0.10} _{-0.08}	0.90 ^{+0.33} _{-0.40}	0.18 ^{+0.06} _{-0.07}	29.4 ^{+2.5} _{-1.7}	0.69 ^{+0.04} _{-0.04}	14000	13.1 ^{+0.2} _{-0.3}
GW190719_215514	55.8 ^{+16.3} _{-10.0}	22.7 ^{+5.9} _{-3.7}	35.2 ^{+16.9} _{-9.9}	20.2 ^{+8.1} _{-6.5}	0.35 ^{+0.28} _{-0.32}	4.61 ^{+2.84} _{-2.17}	0.73 ^{+0.35} _{-0.30}	52.9 ^{+15.6} _{-9.5}	0.80 ^{+0.10} _{-0.16}	2300	8.3 ^{+0.3} _{-1.0}
GW190720_000836	21.3 ^{+4.3} _{-2.3}	8.9 ^{+0.5} _{-0.8}	13.3 ^{+6.6} _{-3.0}	7.8 ^{+2.2} _{-2.2}	0.18 ^{+0.14} _{-0.12}	0.81 ^{+0.71} _{-0.33}	0.16 ^{+0.12} _{-0.06}	20.3 ^{+4.5} _{-2.3}	0.72 ^{+0.06} _{-0.05}	510	11.0 ^{+0.3} _{-0.8}
GW190727_060333	65.8 ^{+10.9} _{-7.4}	28.1 ^{+4.9} _{-3.4}	37.2 ^{+9.4} _{-5.9}	28.8 ^{+6.6} _{-7.9}	0.12 ^{+0.26} _{-0.25}	3.60 ^{+1.56} _{-1.51}	0.60 ^{+0.20} _{-0.22}	62.6 ^{+10.2} _{-7.0}	0.73 ^{+0.10} _{-0.10}	860	11.9 ^{+0.3} _{-0.5}
GW190728_064510	20.5 ^{+4.5} _{-1.3}	8.6 ^{+0.5} _{-0.3}	12.2 ^{+7.1} _{-2.2}	8.1 ^{+1.7} _{-2.6}	0.12 ^{+0.19} _{-0.07}	0.89 ^{+0.25} _{-0.37}	0.18 ^{+0.05} _{-0.07}	19.5 ^{+4.6} _{-1.3}	0.71 ^{+0.04} _{-0.04}	410	13.0 ^{+0.2} _{-0.4}
GW190731_140936	67.1 ^{+15.3} _{-10.2}	28.4 ^{+6.8} _{-4.5}	39.3 ^{+11.8} _{-8.2}	28.0 ^{+8.9} _{-8.4}	0.08 ^{+0.24} _{-0.24}	3.97 ^{+2.56} _{-2.07}	0.65 ^{+0.32} _{-0.30}	63.9 ^{+14.4} _{-9.8}	0.71 ^{+0.10} _{-0.12}	3000	8.6 ^{+0.2} _{-0.5}
GW190803_022701	62.7 ^{+11.8} _{-8.4}	26.7 ^{+5.2} _{-3.8}	36.1 ^{+10.2} _{-6.7}	26.7 ^{+7.1} _{-7.6}	-0.01 ^{+0.25} _{-0.26}	3.69 ^{+2.04} _{-1.69}	0.61 ^{+0.26} _{-0.24}	59.9 ^{+11.2} _{-7.9}	0.69 ^{+0.10} _{-0.11}	1500	8.6 ^{+0.3} _{-0.5}
GW190814	25.8 ^{+1.0} _{-0.9}	6.09 ^{+0.06} _{-0.06}	23.2 ^{+1.1} _{-1.0}	2.59 ^{+0.08} _{-0.09}	0.00 ^{+0.06} _{-0.06}	0.24 ^{+0.04} _{-0.05}	0.05 ^{+0.009} _{-0.010}	25.6 ^{+1.0} _{-0.9}	0.28 ^{+0.02} _{-0.02}	19	24.9 ^{+0.1} _{-0.2}
GW190828_063405	57.5 ^{+7.5} _{-4.4}	24.8 ^{+3.3} _{-2.0}	31.8 ^{+5.8} _{-3.9}	25.9 ^{+4.4} _{-4.6}	0.19 ^{+0.15} _{-0.16}	2.22 ^{+0.63} _{-0.95}	0.40 ^{+0.09} _{-0.15}	54.5 ^{+6.9} _{-4.0}	0.76 ^{+0.06} _{-0.07}	520	16.2 ^{+0.2} _{-0.3}
GW190828_065509	34.1 ^{+5.5} _{-4.5}	13.3 ^{+1.2} _{-0.9}	23.8 ^{+7.2} _{-7.0}	10.2 ^{+3.5} _{-2.1}	0.08 ^{+0.16} _{-0.16}	1.66 ^{+0.63} _{-0.61}	0.31 ^{+0.10} _{-0.10}	32.9 ^{+5.7} _{-4.5}	0.65 ^{+0.09} _{-0.08}	640	10.0 ^{+0.3} _{-0.5}
GW190909_114149	71.2 ^{+54.3} _{-15.0}	29.5 ^{+17.5} _{-12.2}	43.2 ^{+50.7} _{-10.9}	27.6 ^{+13.0} _{-10.9}	-0.03 ^{+0.44} _{-0.36}	4.77 ^{+3.70} _{-2.66}	0.75 ^{+0.45} _{-0.37}	68.3 ^{+52.5} _{-14.5}	0.68 ^{+0.16} _{-0.18}	4200	8.1 ^{+0.4} _{-0.7}
GW190910_112807	78.7 ^{+9.5} _{-9.0}	33.9 ^{+4.3} _{-3.9}	43.5 ^{+7.6} _{-6.2}	35.1 ^{+6.3} _{-7.0}	0.02 ^{+0.19} _{-0.18}	1.57 ^{+1.07} _{-0.64}	0.29 ^{+0.17} _{-0.11}	75.0 ^{+8.7} _{-8.5}	0.70 ^{+0.08} _{-0.07}	10000	14.1 ^{+0.2} _{-0.3}
GW190915_235702	59.5 ^{+7.5} _{-6.2}	25.1 ^{+3.1} _{-2.6}	34.9 ^{+9.5} _{-6.2}	24.4 ^{+5.5} _{-6.0}	0.03 ^{+0.19} _{-0.24}	1.70 ^{+0.71} _{-0.64}	0.32 ^{+0.11} _{-0.11}	56.8 ^{+7.1} _{-5.8}	0.71 ^{+0.09} _{-0.11}	380	13.6 ^{+0.2} _{-0.3}
GW190924_021846	13.9 ^{+5.1} _{-0.9}	5.8 ^{+0.2} _{-0.2}	8.8 ^{+7.0} _{-2.0}	5.0 ^{+1.3} _{-1.9}	0.03 ^{+0.30} _{-0.09}	0.57 ^{+0.22} _{-0.22}	0.12 ^{+0.04} _{-0.04}	13.3 ^{+5.2} _{-1.0}	0.67 ^{+0.05} _{-0.05}	380	11.5 ^{+0.3} _{-0.4}
GW190929_012149	90.6 ^{+21.2} _{-14.1}	34.3 ^{+8.6} _{-6.5}	64.7 ^{+22.4} _{-18.9}	25.7 ^{+14.4} _{-9.7}	0.03 ^{+0.27} _{-0.27}	3.68 ^{+2.98} _{-1.68}	0.61 ^{+0.38} _{-0.24}	87.5 ^{+20.7} _{-14.1}	0.64 ^{+0.17} _{-0.23}	1800	9.8 ^{+0.8} _{-0.6}
GW190930_133541	20.3 ^{+9.0} _{-1.5</}										



GW190412 : asymmetric masses

PRD 102 (2020) 043015

TABLE II. Inferred parameter values for GW190412 and their 90% credible intervals, obtained using precessing models including higher multipoles.

Parameter ^a	EOBNR PHM	Phenom PHM	Combined
m_1/M_\odot	$31.7^{+3.6}_{-3.5}$	$28.1^{+4.8}_{-4.3}$	$30.1^{+4.6}_{-5.3}$
m_2/M_\odot	$8.0^{+0.9}_{-0.7}$	$8.8^{+1.6}_{-1.1}$	$8.3^{+1.6}_{-0.9}$
M/M_\odot	$39.7^{+3.0}_{-2.8}$	$36.9^{+3.7}_{-2.9}$	$38.4^{+3.8}_{-3.9}$
\mathcal{M}/M_\odot	$13.3^{+0.3}_{-0.3}$	$13.2^{+0.5}_{-0.3}$	$13.3^{+0.4}_{-0.4}$
q	$0.25^{+0.06}_{-0.04}$	$0.31^{+0.12}_{-0.07}$	$0.28^{+0.12}_{-0.07}$
M_f/M_\odot	$38.6^{+3.1}_{-2.8}$	$35.7^{+3.8}_{-3.0}$	$37.3^{+3.8}_{-4.0}$
χ_f	$0.68^{+0.04}_{-0.04}$	$0.67^{+0.07}_{-0.07}$	$0.67^{+0.06}_{-0.05}$
m_1^{det}/M_\odot	$36.5^{+4.2}_{-4.2}$	$32.3^{+5.7}_{-5.2}$	$34.6^{+5.4}_{-6.4}$
m_2^{det}/M_\odot	$9.2^{+0.9}_{-0.7}$	$10.1^{+1.6}_{-1.2}$	$9.6^{+1.7}_{-1.0}$
M^{det}/M_\odot	$45.7^{+3.5}_{-3.3}$	$42.5^{+4.4}_{-3.7}$	$44.2^{+4.4}_{-4.7}$
$\mathcal{M}^{\text{det}}/M_\odot$	$15.3^{+0.1}_{-0.2}$	$15.2^{+0.3}_{-0.2}$	$15.2^{+0.3}_{-0.1}$
χ_{eff}	$0.28^{+0.06}_{-0.08}$	$0.22^{+0.08}_{-0.11}$	$0.25^{+0.08}_{-0.11}$
χ_p	$0.31^{+0.14}_{-0.15}$	$0.31^{+0.24}_{-0.17}$	$0.31^{+0.19}_{-0.16}$
χ_1	$0.46^{+0.12}_{-0.15}$	$0.41^{+0.22}_{-0.24}$	$0.44^{+0.16}_{-0.22}$
D_L/Mpc	740^{+120}_{-130}	740^{+150}_{-190}	740^{+130}_{-160}
z	$0.15^{+0.02}_{-0.02}$	$0.15^{+0.03}_{-0.04}$	$0.15^{+0.03}_{-0.03}$
$\hat{\theta}_{JN}$	$0.71^{+0.23}_{-0.21}$	$0.71^{+0.39}_{-0.27}$	$0.71^{+0.31}_{-0.24}$
ρ_H	$9.5^{+0.1}_{-0.2}$	$9.5^{+0.2}_{-0.3}$	$9.5^{+0.1}_{-0.3}$
ρ_L	$16.2^{+0.1}_{-0.2}$	$16.1^{+0.2}_{-0.3}$	$16.2^{+0.1}_{-0.3}$
ρ_V	$3.7^{+0.2}_{-0.5}$	$3.6^{+0.3}_{-0.7}$	$3.6^{+0.3}_{-0.7}$
ρ_{HLV}	$19.1^{+0.2}_{-0.2}$	$19.0^{+0.2}_{-0.3}$	$19.1^{+0.1}_{-0.3}$

mass $30.1^{+4.6}_{-5.3} M_{\text{sun}} + 8.3^{+1.6}_{-0.9} M_{\text{sun}} \rightarrow 37.3^{+3.8}_{-4.0} M_{\text{sun}}$
distance $740^{+130}_{-160} \text{ Mpc}$, $z = 0.15^{+0.03}_{-0.03}$

$m=3$ modes
are visible!

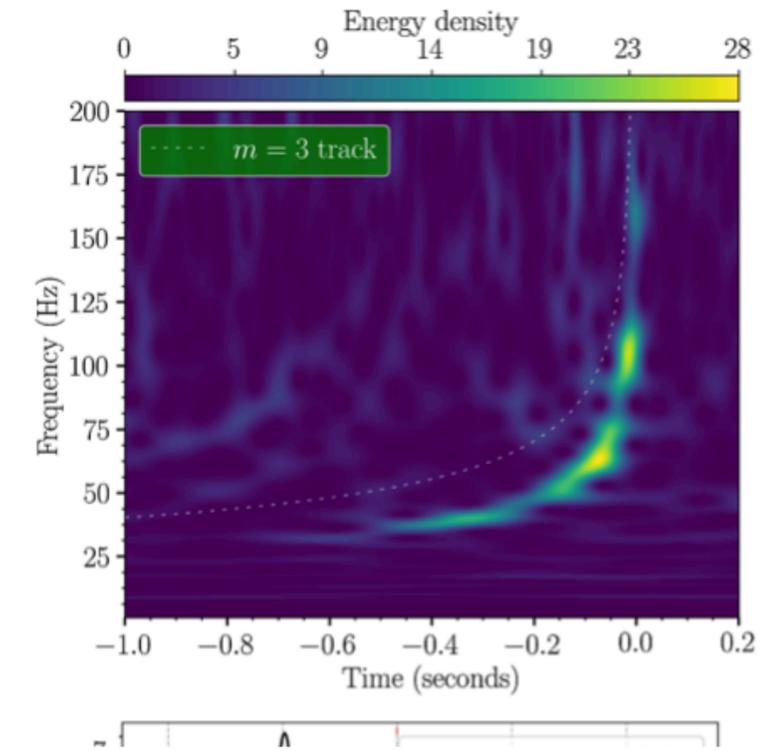


FIG. 8. Top panel: Time-frequency spectrogram of data containing GW190412, observed in the LIGO Livingston detector. The horizontal axis is time (in seconds) relative to the trigger time (1239082262.17). The amplitude scale of the detector output is normalized by the PSD of the noise. To illustrate the method, the predicted track for the $m = 3$ multipoles is highlighted as a dashed line, above the track from the $m = 2$ multipoles that are visible in the spectrogram. Bottom panel: The variation of $Y(\alpha)$, i.e., the energy in the pixels of the top panel, along the track defined by $f_\alpha(t) = \alpha f_{22}(t)$, where $f_{22}(t)$ is computed from the Phenom HM analysis. Two consecutive peaks at $\alpha = 1.0$ and $\alpha = 1.5$ (thin dashed line) indicate the energy of the $m = 2$ and $m = 3$ multipoles, respectively. Inset: The distribution of the detection statistic β in noise, used to quantify p -values for the hypothesis that the data contains $m = 2$ and $m = 3$ multipoles (red dashed line).

waveform with modulation

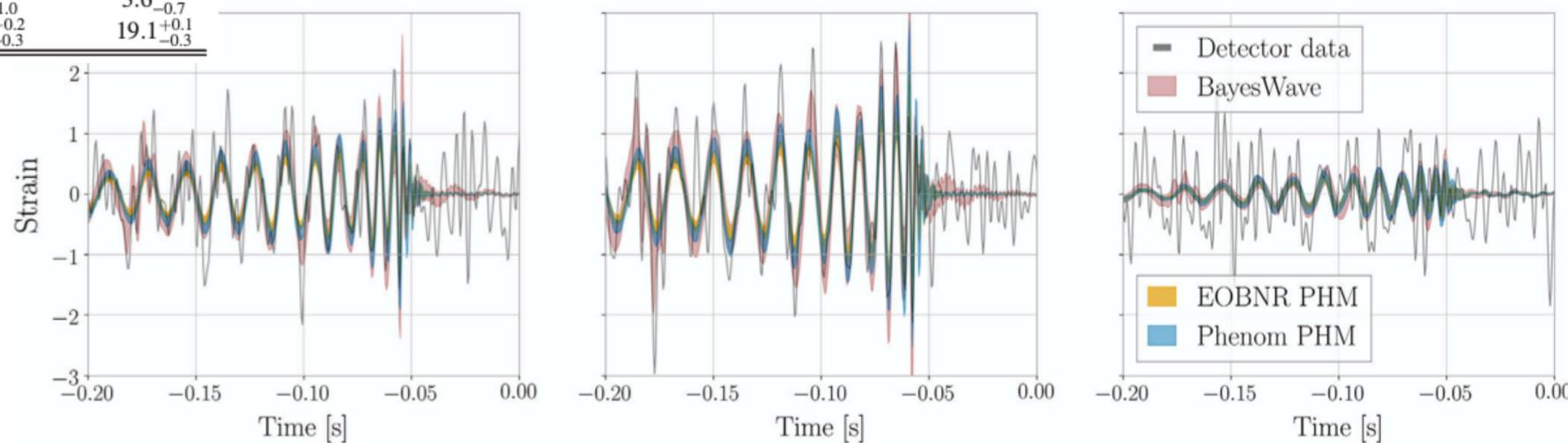


FIG. 9. Reconstructions of the gravitational waveform of GW190412 in the LIGO Hanford, LIGO Livingston and Virgo detectors (from left to right). We show detector data, whitened by an inverse amplitude-spectral-density filter computed using BayesLine [105], together with the unmodeled BayesWave reconstruction that uses a wavelet bases, and the reconstruction based on the precessing, higher multipole models from the EOBNR and Phenom families. The bands indicate the 90% credible intervals at each time. We caution that some apparent amplitude fluctuations in this figure are an artifact of the whitening procedure.

GW190521 Largest BH ever (1)

PRL 125 (2020) 101102

PHYSICAL REVIEW LETTERS **125**, 101102 (2020)

Editors' Suggestion Featured in Physics

GW190521: A Binary Black Hole Merger with a Total Mass of $150 M_{\odot}$

R. Abbott *et al.*^{*}
(LIGO Scientific Collaboration and Virgo Collaboration)

(Received 30 May 2020; revised 19 June 2020; accepted 9 July 2020; published 2 September 2020; corrected 23 October 2020)

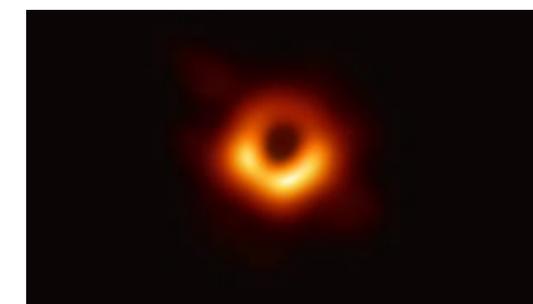
On May 21, 2019 at 03:02:29 UTC Advanced LIGO and Advanced Virgo observed a short duration gravitational-wave signal, GW190521, with a three-detector network signal-to-noise ratio of 14.7, and an estimated false-alarm rate of 1 in 4900 yr using a search sensitive to generic transients. If GW190521 is from a quasicircular binary inspiral, then the detected signal is consistent with the merger of two black holes with masses of $85^{+21}_{-14} M_{\odot}$ and $66^{+17}_{-18} M_{\odot}$ (90% credible intervals). We infer that the primary black hole mass lies within the gap produced by (pulsational) pair-instability supernova processes, with only a 0.32% probability of being below $65 M_{\odot}$. We calculate the mass of the remnant to be $142^{+28}_{-16} M_{\odot}$, which can be considered an intermediate mass black hole (IMBH). The luminosity distance of the source is $5.3^{+2.4}_{-2.6}$ Gpc, corresponding to a redshift of $0.82^{+0.28}_{-0.34}$. The inferred rate of mergers similar to GW190521 is $0.13^{+0.30}_{-0.11} \text{ Gpc}^{-3} \text{ yr}^{-1}$.

mass $85^{+21}_{-14} M_{\text{sun}} + 66^{+17}_{-18} M_{\text{sun}} \rightarrow 142^{+28}_{-16} M_{\text{sun}}$
 distance $5.3^{+2.4}_{-2.6} \text{ Gpc}, z = 0.82^{+0.28}_{-0.34}$

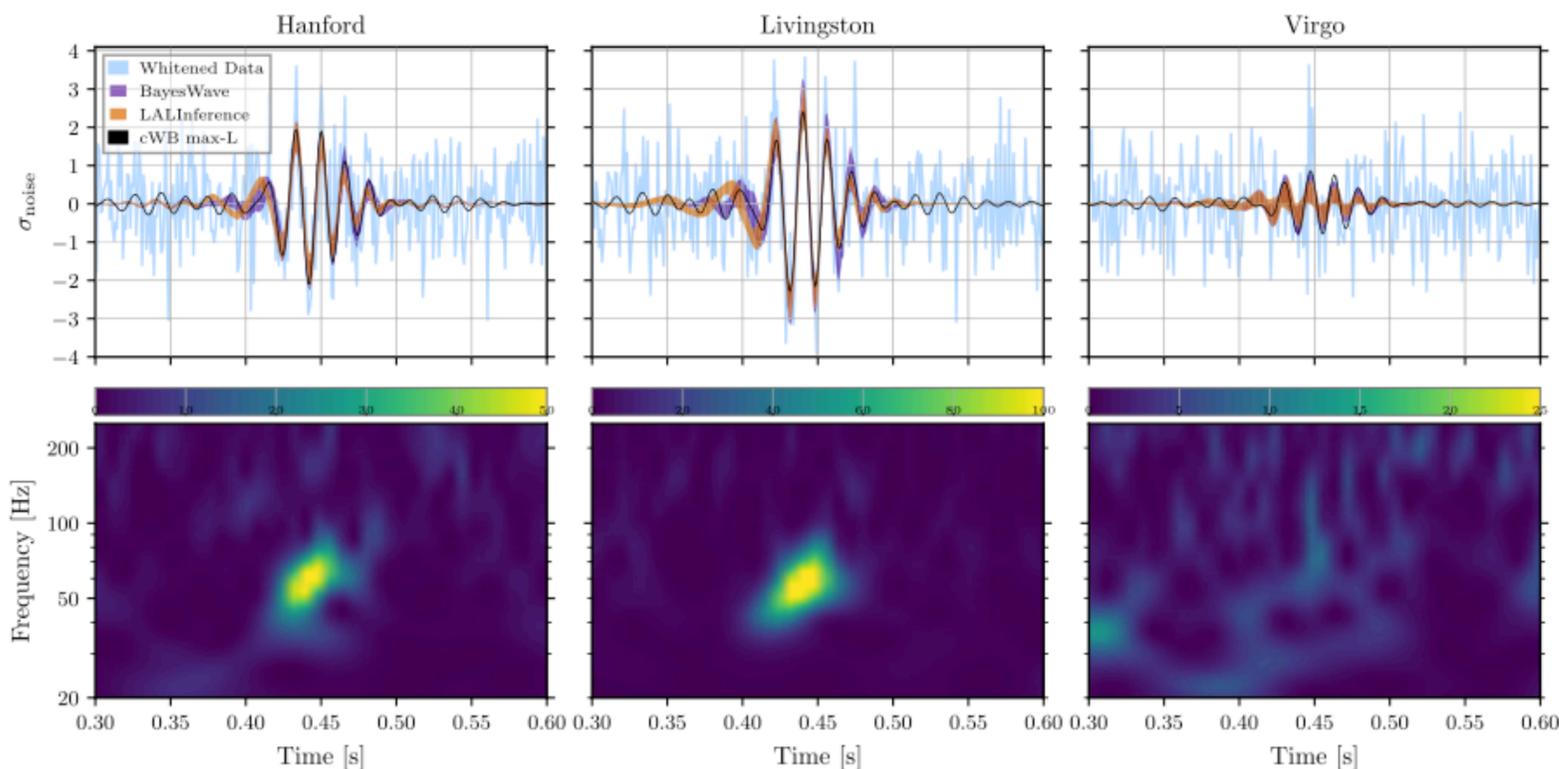


Discovery of IMBH over $100 M_{\text{sun}}$

no formation route of BH over $65 M_{\text{sun}}$

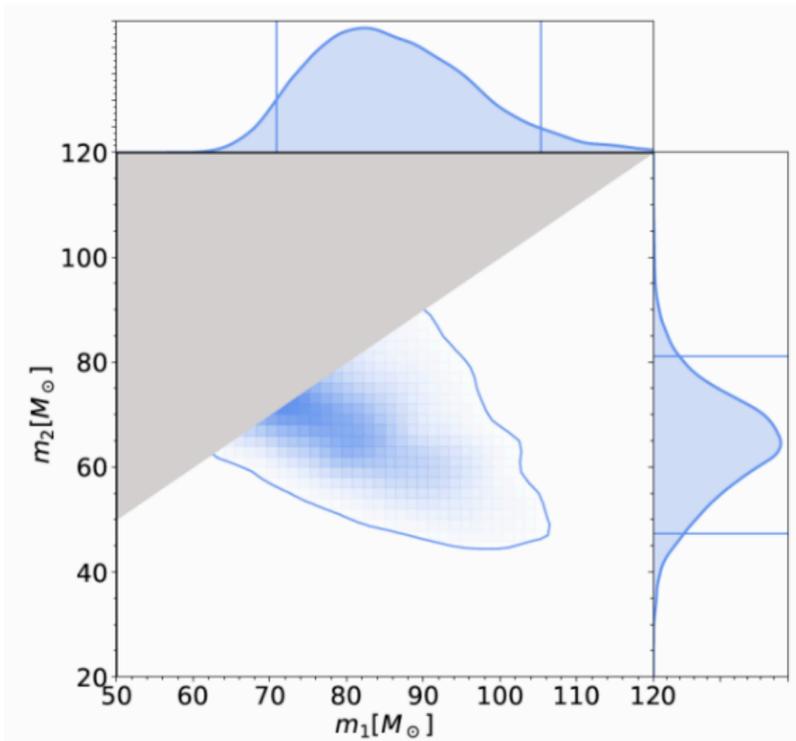


M87 by EHT
 mass $0.65 G M_{\text{sun}}$
 dist. 55 M ly
 16.9 Mpc

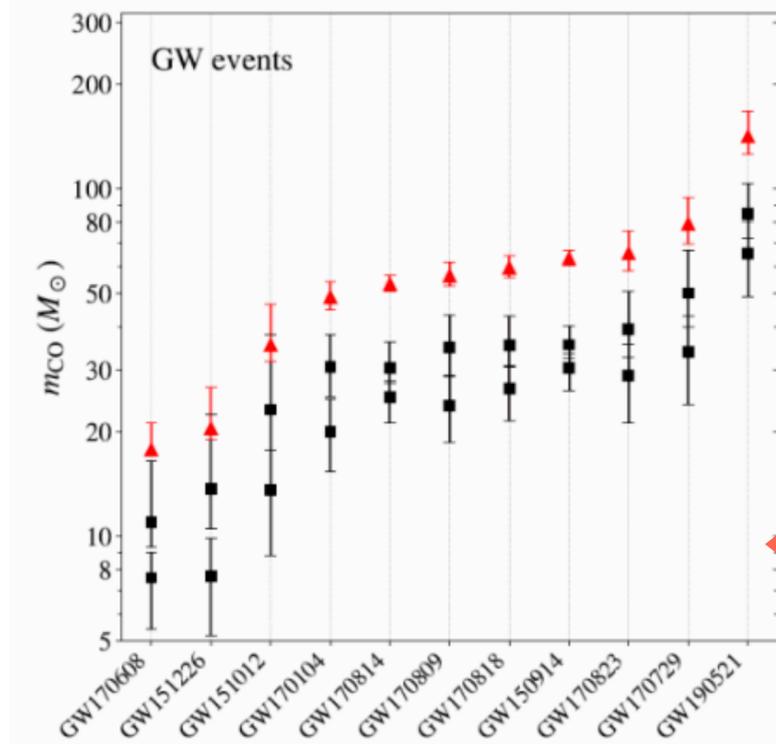


GW190521 Largest BH ever (2)

PRL 125 (2020) 101102



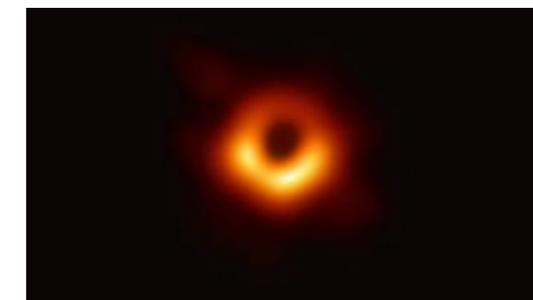
mass $85^{+21}_{-14} M_{\text{sun}} + 66^{+17}_{-18} M_{\text{sun}} \rightarrow 142^{+28}_{-16} M_{\text{sun}}$
 distance $5.3^{+2.4}_{-2.6} \text{ Gpc}, z = 0.82^{+0.28}_{-0.34}$



Discovery of IMBH over 100 M_{sun}

no formation route of BH over 65 M_{sun}

second generation of BBH



M87 by EHT
 mass $0.65 G M_{\text{sun}}$
 dist. 55 M ly
 16.9 Mpc

[Submitted on 14 Jan 2021]

Alternative possibility of GW190521: Gravitational waves from high-mass black hole-disk systems

Masaru Shibata, Kenta Kiuchi, Sho Fujibayashi, Yuichiro Sekiguchi

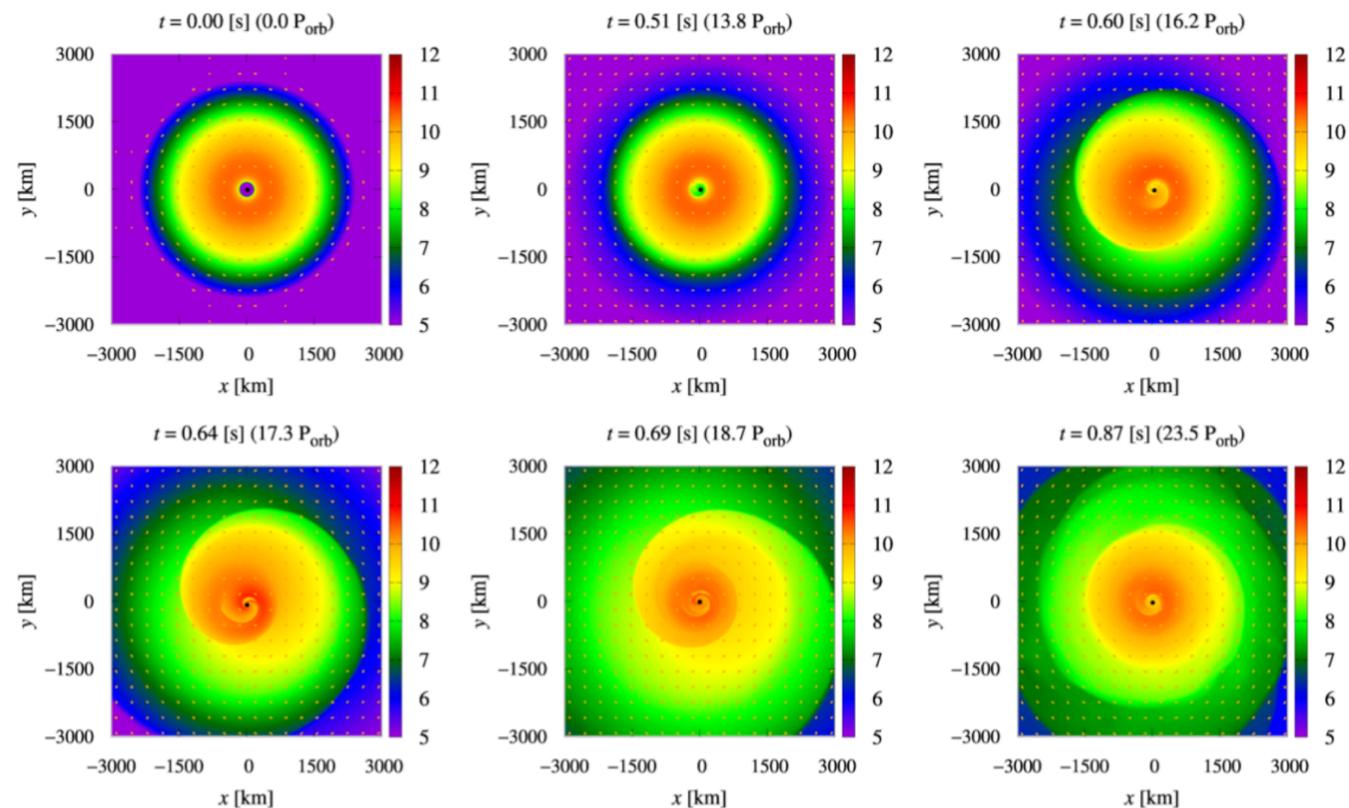
We evolve high-mass disks of mass $15 - 50M_{\odot}$ orbiting a $50M_{\odot}$ spinning black hole in the framework of numerical relativity. Such high-mass systems could be an outcome during the collapse of rapidly-rotating very-massive stars. The massive disks are dynamically unstable to the so-called one-armed spiral-shape deformation with the maximum fractional density-perturbation of $\delta\rho/\rho \gtrsim 0.1$, and hence, high-amplitude gravitational waves are emitted. The waveforms are characterized by an initial high-amplitude burst with the frequency of $\sim 40 - 50$ Hz and the maximum amplitude of $(1 - 10) \times 10^{-22}$ at the hypothetical distance of 100 Mpc and by a subsequent low-amplitude quasi-periodic oscillation. We illustrate that the waveforms in our models with a wide range of the disk mass resemble that of GW190521. We also point out that gravitational waves from rapidly-rotating very-massive stars can be the source for 3rd-generation gravitational-wave detectors for exploring the formation process of rapidly-rotating high-mass black holes of mass $\sim 50 - 100M_{\odot}$ in an early universe.

GW190521

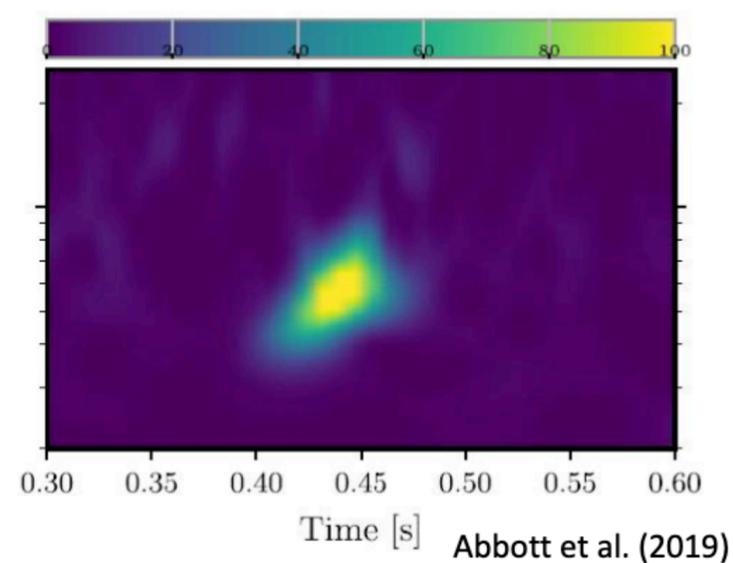
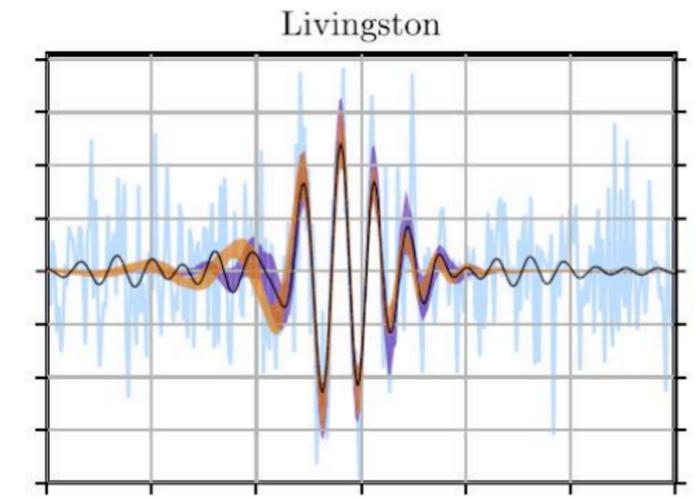
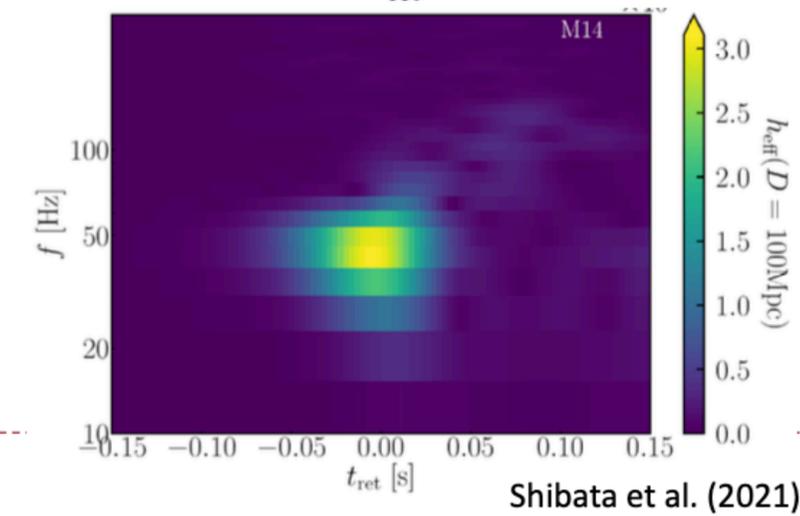
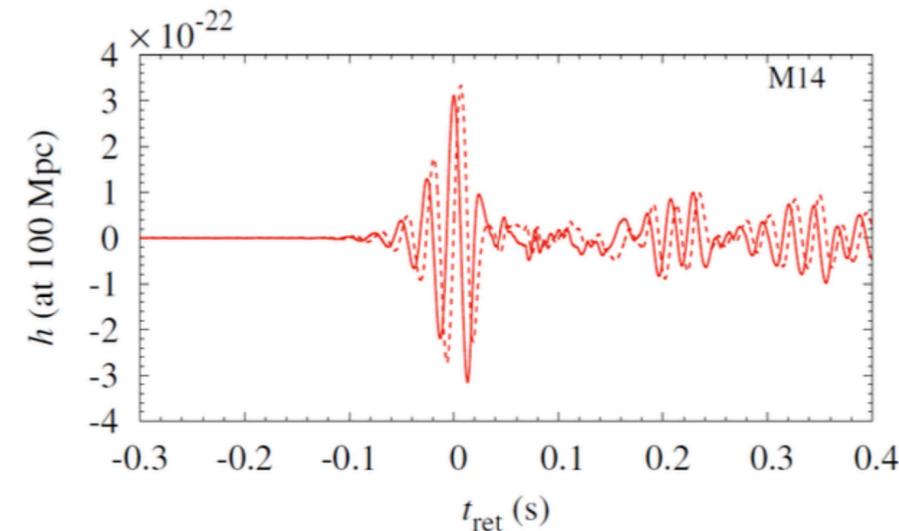
質量 $85^{+21}_{-14} M_{\text{sun}} + 66^{+17}_{-18} M_{\text{sun}} \rightarrow 142^{+28}_{-16} M_{\text{sun}}$

距離 $5.3^{+2.4}_{-2.6}$ Gpc, $z = 0.82^{+0.28}_{-0.34}$

50 M_{sun} BH + 30 M_{sun} Disk



GW from one-armed spiral instability



GW190814 : 23M + 2.6M

ApJL 896 (2020) L44

mass $23.2^{+1.1}_{-1.0} M_{\text{sun}} + 2.59^{+0.08}_{-0.09} M_{\text{sun}} \rightarrow 25.6^{+1.1}_{-0.9} M_{\text{sun}}$ distance $241^{+41}_{-45} \text{ Mpc}$, $z = 0.053^{+0.009}_{-0.010}$

Table 1
Source Properties of GW190814: We Report the Median Values Along with the Symmetric 90% Credible Intervals for the SEOBNRv4PHM (EOBNR PHM) and IMRPHENOMPv3HM (PHENOM PHM) Waveform Models

	EOBNR PHM	Phenom PHM	Combined
Primary mass m_1/M_{\odot}	$23.2^{+1.0}_{-0.9}$	$23.2^{+1.3}_{-1.1}$	$23.2^{+1.1}_{-1.0}$
Secondary mass m_2/M_{\odot}	$2.59^{+0.08}_{-0.08}$	$2.58^{+0.09}_{-0.10}$	$2.59^{+0.08}_{-0.09}$
Mass ratio q	$0.112^{+0.008}_{-0.008}$	$0.111^{+0.009}_{-0.010}$	$0.112^{+0.008}_{-0.009}$
Chirp mass \mathcal{M}/M_{\odot}	$6.10^{+0.06}_{-0.05}$	$6.08^{+0.06}_{-0.05}$	$6.09^{+0.06}_{-0.06}$
Total mass M/M_{\odot}	$25.8^{+0.9}_{-0.8}$	$25.8^{+1.2}_{-1.0}$	$25.8^{+1.0}_{-0.9}$
Final mass M_f/M_{\odot}	$25.6^{+1.0}_{-0.8}$	$25.5^{+1.2}_{-1.0}$	$25.6^{+1.1}_{-0.9}$
Upper bound on primary spin magnitude χ_1	0.06	0.08	0.07
Effective inspiral spin parameter χ_{eff}	$0.001^{+0.059}_{-0.056}$	$-0.005^{+0.061}_{-0.065}$	$-0.002^{+0.060}_{-0.061}$
Upper bound on effective precession parameter χ_p	0.07	0.07	0.07
Final spin χ_f	$0.28^{+0.02}_{-0.02}$	$0.28^{+0.02}_{-0.03}$	$0.28^{+0.02}_{-0.02}$
Luminosity distance D_L/Mpc	235^{+40}_{-45}	249^{+39}_{-43}	241^{+41}_{-45}
Source redshift z	$0.051^{+0.008}_{-0.009}$	$0.054^{+0.008}_{-0.009}$	$0.053^{+0.009}_{-0.010}$
Inclination angle Θ/rad	$0.9^{+0.3}_{-0.2}$	$0.8^{+0.3}_{-0.2}$	$0.8^{+0.3}_{-0.2}$
Signal-to-noise ratio in LIGO Hanford ρ_H	$10.6^{+0.1}_{-0.1}$	$10.7^{+0.1}_{-0.2}$	$10.7^{+0.1}_{-0.2}$
Signal-to-noise ratio in LIGO Livingston ρ_L	$22.21^{+0.09}_{-0.15}$	$22.16^{+0.09}_{-0.17}$	$22.18^{+0.10}_{-0.17}$
Signal-to-noise ratio in Virgo ρ_V	$4.3^{+0.2}_{-0.5}$	$4.1^{+0.2}_{-0.6}$	$4.2^{+0.2}_{-0.6}$
Network Signal-to-noise ratio ρ_{HLV}	$25.0^{+0.1}_{-0.2}$	$24.9^{+0.1}_{-0.2}$	$25.0^{+0.1}_{-0.2}$

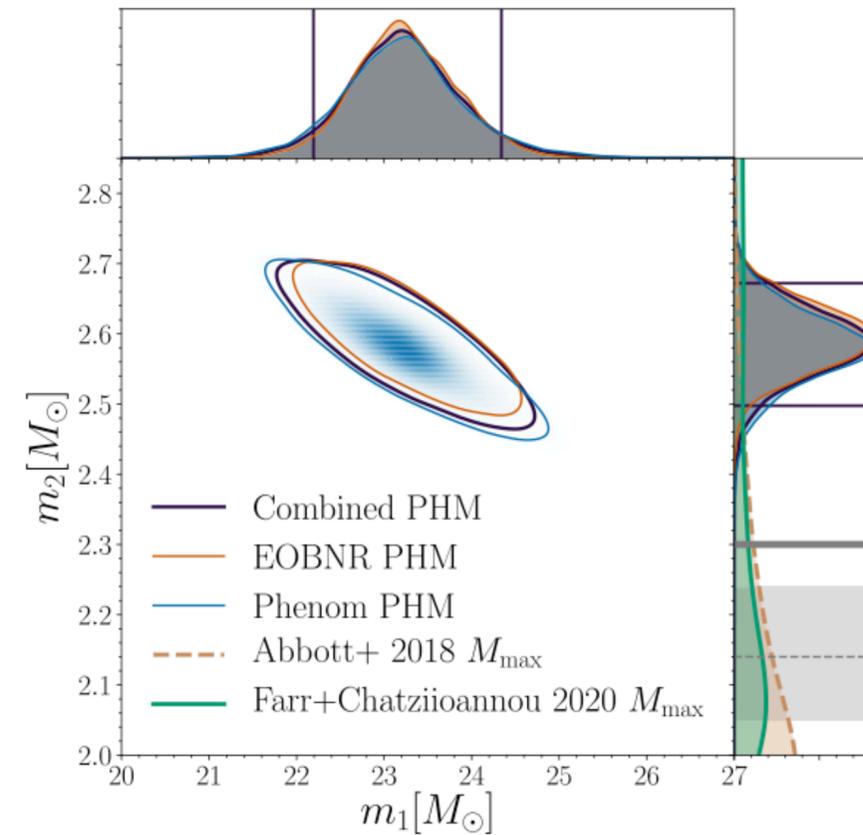
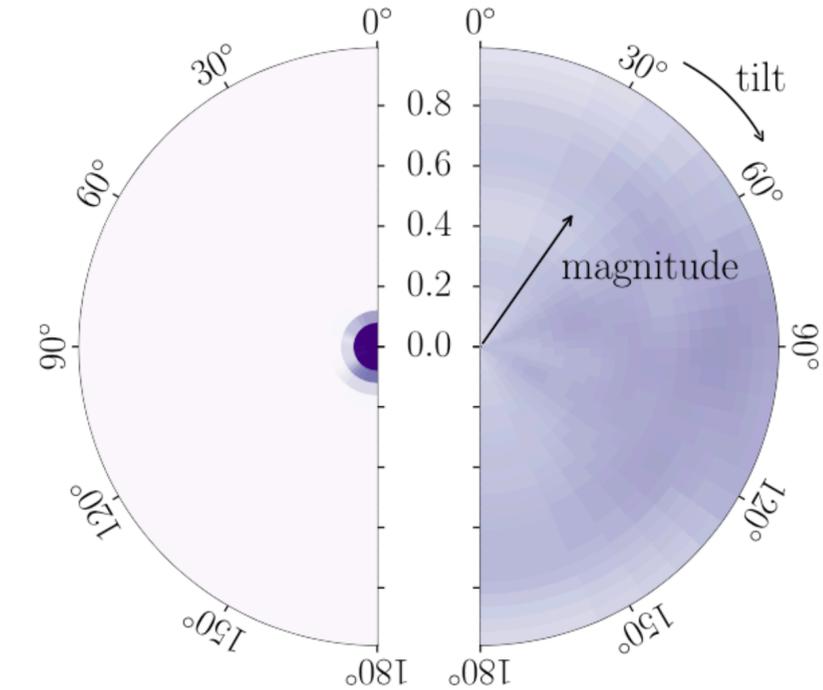
mass ratio $q=0.11$ primary (BH)
spin = 0secondary
spin = ?

Figure 6. Two-dimensional posterior probability for the tilt-angle and spin-magnitude for the primary object (left) and secondary object (right) based on the combined samples. The tilt angles are 0° for spins aligned and 180° for spins antialigned with the orbital angular momentum. The tiles are constructed linearly in spin magnitude and the cosine of the tilt angles such that each tile contains identical prior probability. The color indicates the posterior probability per pixel. The probabilities are marginalized over the azimuthal angles.

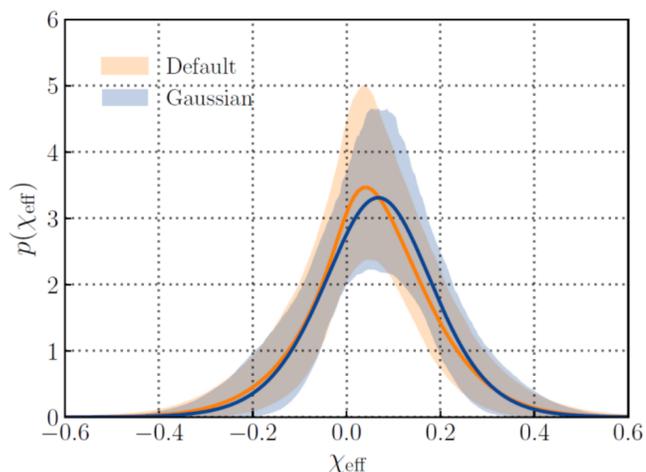
secondary component is either the lightest BH or the heaviest NS

GWTC-2 properties

- ★ smallest BH 6 M_{sun} or 2.6 M_{sun}
GW190814 (23 M_{sun} + 2.6 M_{sun}) BH+BH or BH+NS
- ★ largest BH 150 M_{sun}
GW190521 (85 M_{sun} + 66 M_{sun})
- ★ BBH with large mass ratio
GW190412 (30 M_{sun} + 8.3 M_{sun}) & GW190814
- ★ BBH with negative effective spin

Is 2.6 M_{sun} object is NS or BH?

Evidence of dynamical formation ?



$$\chi_{\text{eff}} = \frac{1}{M} \left(\frac{\vec{S}_1}{m_1} + \frac{\vec{S}_2}{m_2} \right) \cdot \frac{\vec{L}_N}{\|\vec{L}_N\|}$$

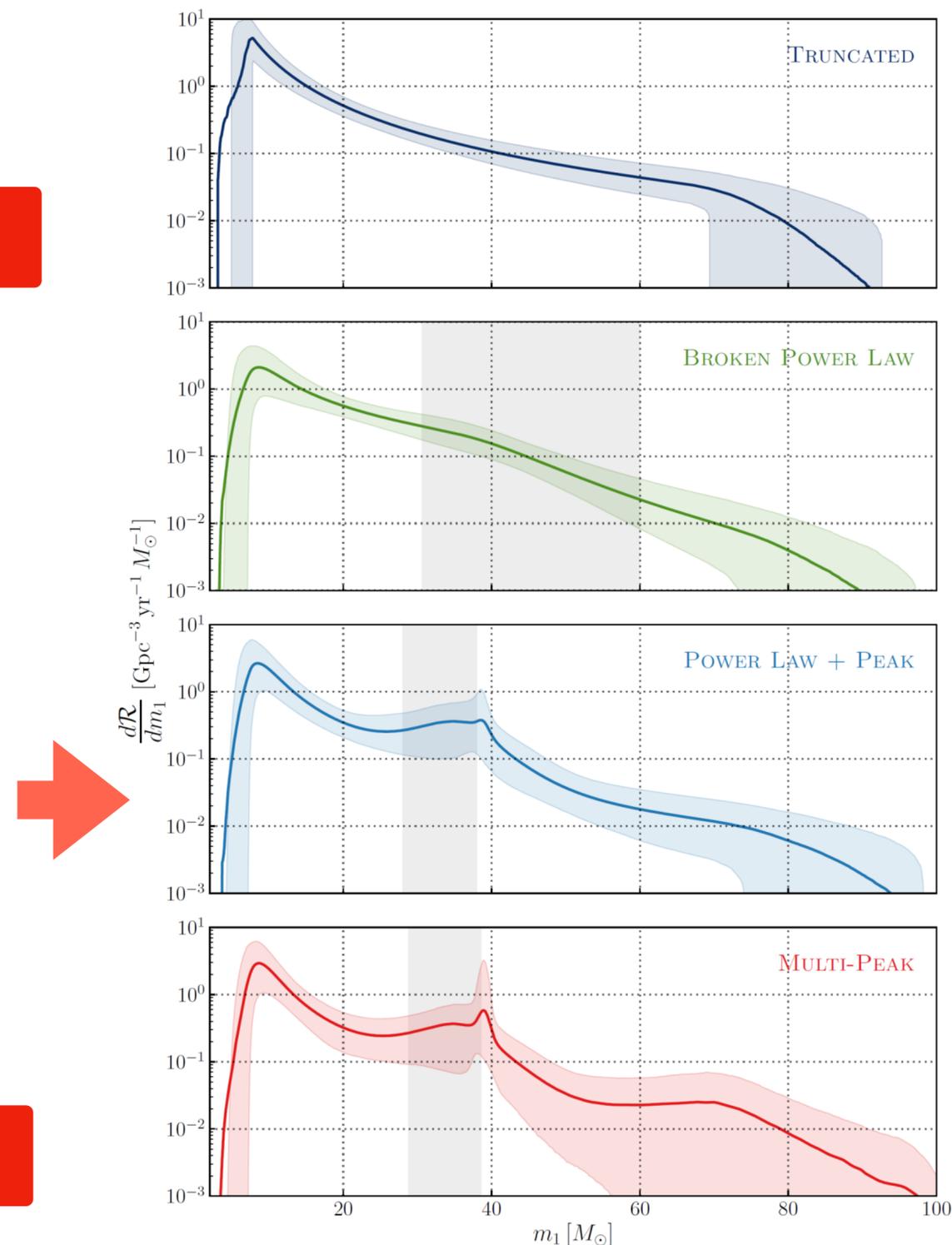
- ★ mass profile of BHs: best fit power with 2.00 ~ 2.73 + one peak at 40Msun

Origin of the peak ?

★ Event Rate

$$\mathcal{R}_{\text{BBH}} = 23.9_{-8.6}^{+14.9} \text{ Gpc}^{-3} \text{ yr}^{-1}$$

$$\mathcal{R}_{\text{BNS}} = 320_{-240}^{+490} \text{ Gpc}^{-3} \text{ yr}^{-1}$$



GW search near GRB events

In O3a, Fermi/Swift detected ~ 150 GRB

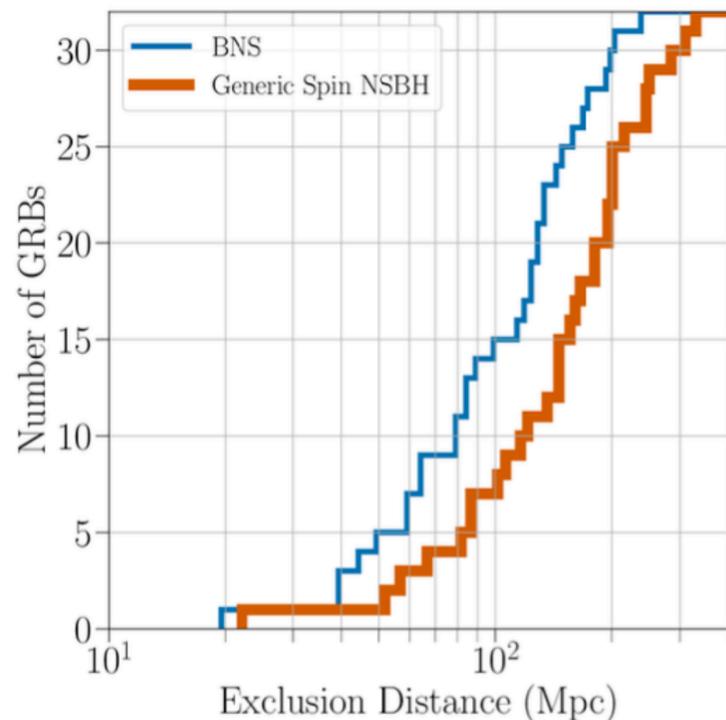
short GRB (ms--s) : NSNS, NSBH (likely for GW170817) ▶ Modeled Search for 32 GRBs

long GRB (s--min) : SN? ▶ Generic Burst Search for 105 GRBs

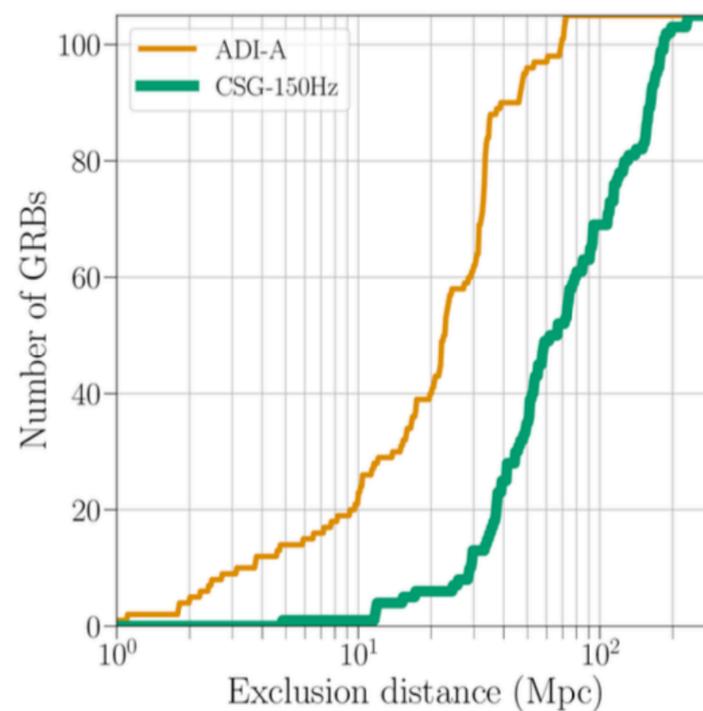
➡ **no GW detection**

distance to GRB source ?

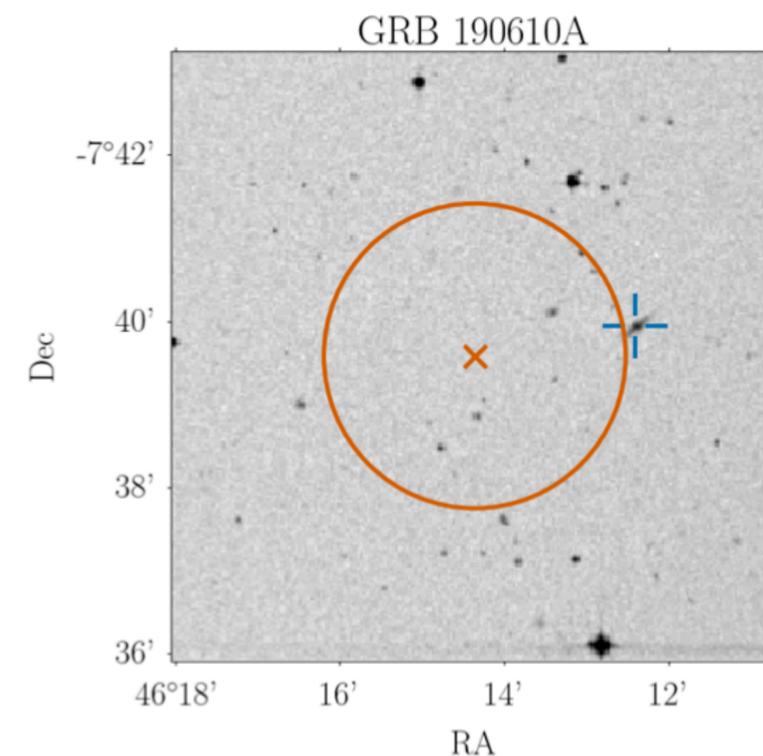
▶ should be away than LIGO-Virgo Obs distance



「Exclusion Distance」 for Modeled Search using chirp signal for 32 GRB events



「Exclusion Distance」 for Burst Search for 105 GRB events

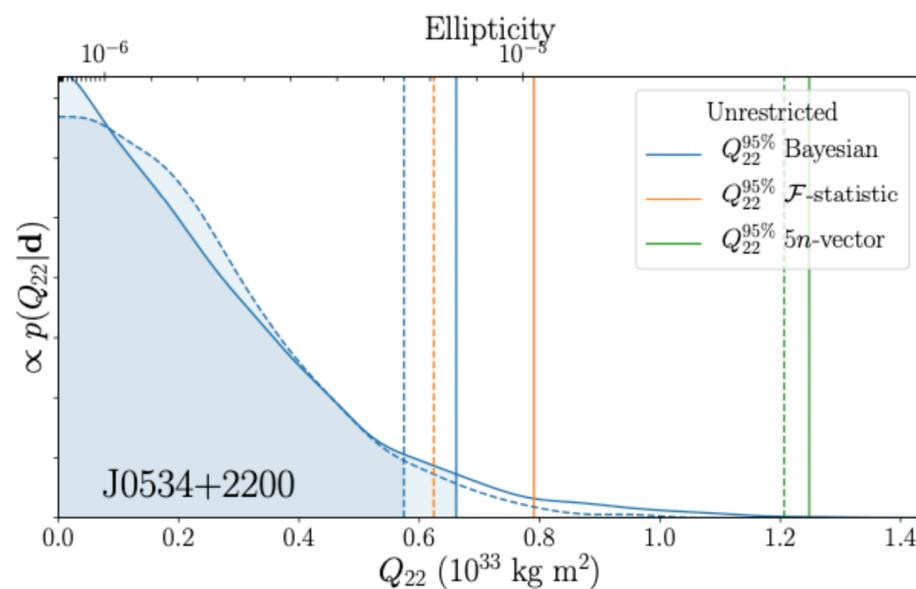
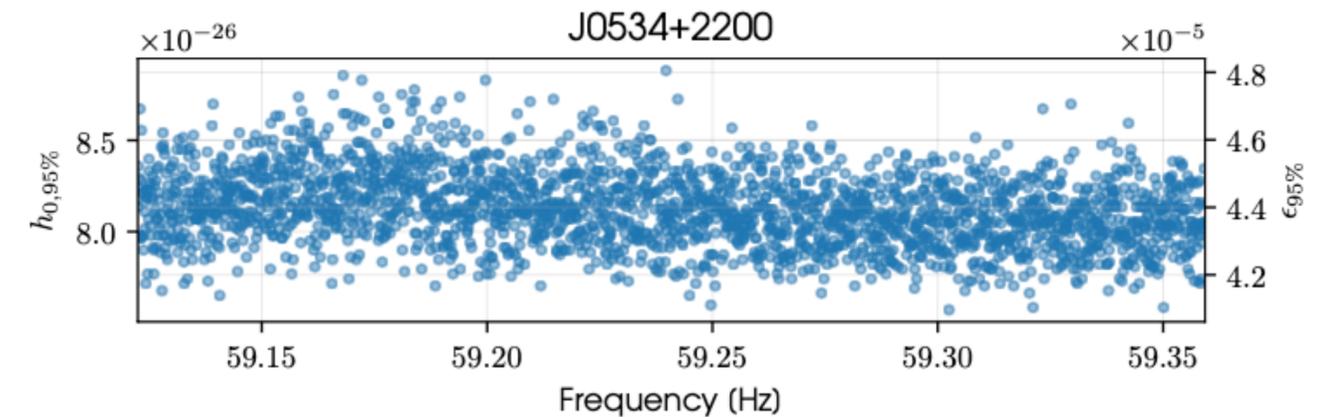
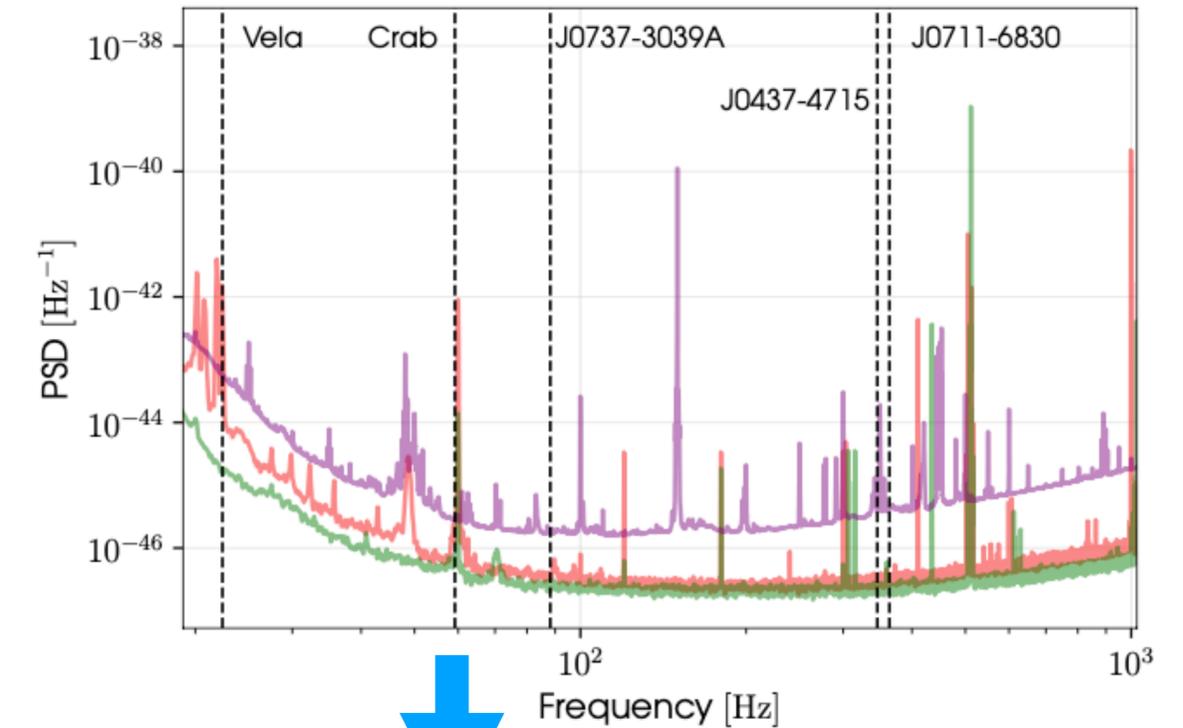


If GRB190610A is NSNS, the distance is over 63 Mpc. Near the source region, there is a galaxy at 165 Mpc. Consistent.

No “mountains” in msec-pulsars

O1+O2+O3a data, GW emission from 5 known pulsars.

Pulsar	f_{rot} (Hz)	\dot{f}_{rot} (Hz s ⁻¹)	$\dot{f}_{\text{rot}}^{\text{int}}$ (Hz s ⁻¹)	distance (kpc)	Spin-down luminosity (W)
Young pulsars					
J0534+2200 (Crab)	29.6	-3.7×10^{-10}	...	2.0 ± 0.5^a	4.5×10^{31}
J0835-4510 (Vela)	11.2	$-2.8 \times 10^{-11}^b$...	$0.287^{+0.019}_-0.017^c$	6.9×10^{29}
Recycled pulsars					
J0437-4715	173.7	-1.7×10^{-15}	-4.1×10^{-16}	0.15679 ± 0.00025^d	2.8×10^{26}
J0711-6830	182.1	-4.9×10^{-16}	-4.7×10^{-16}	0.110 ± 0.044^e	3.4×10^{26}
J0737-3039A	44.1	-3.4×10^{-15}	...	$1.15^{+0.22}_-0.16^f$	5.9×10^{26}



no GW detection

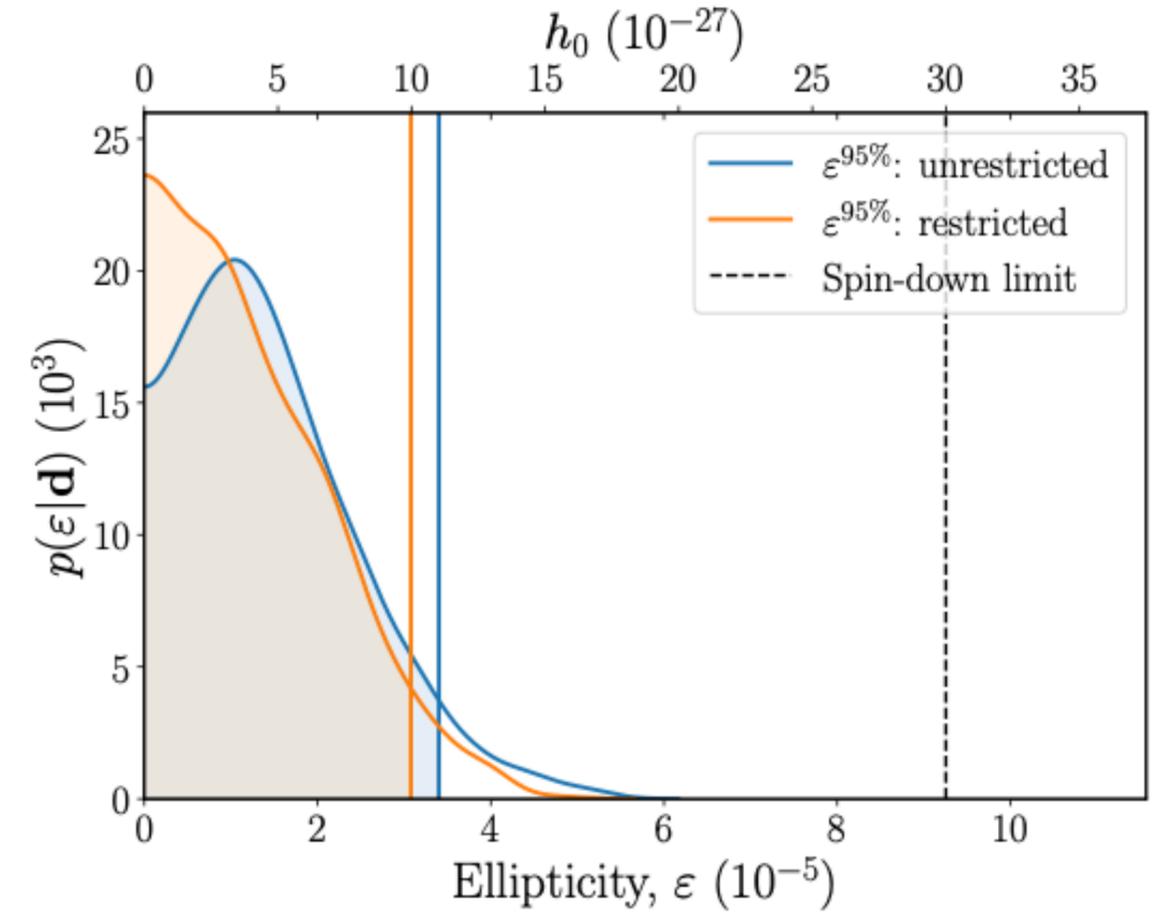
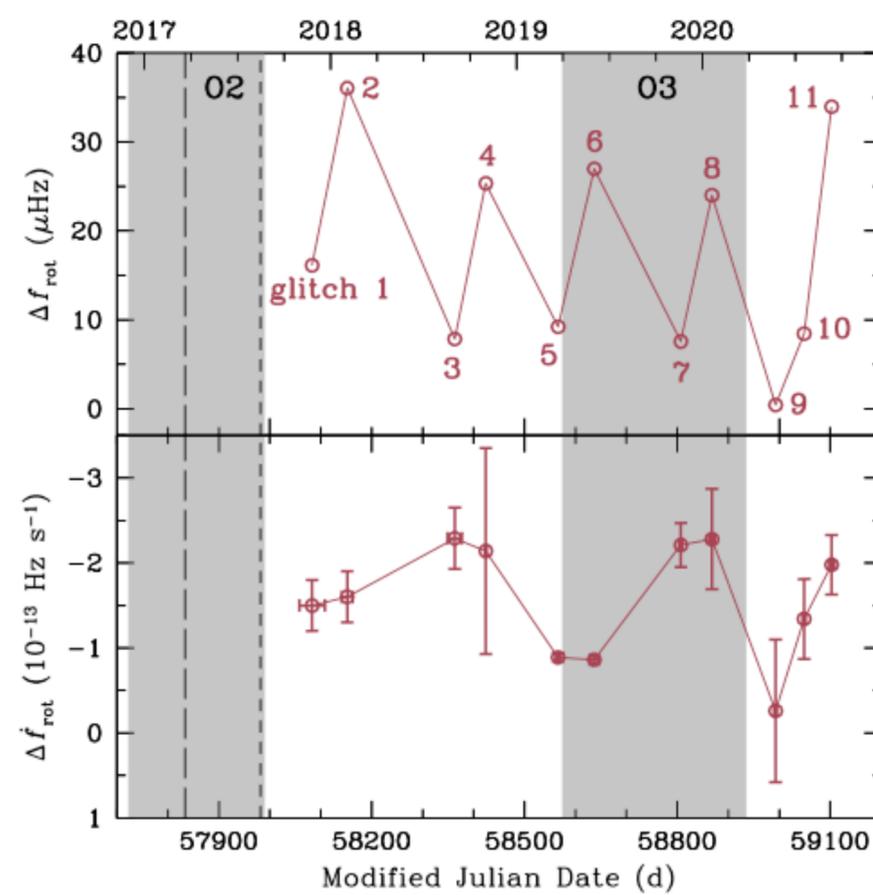
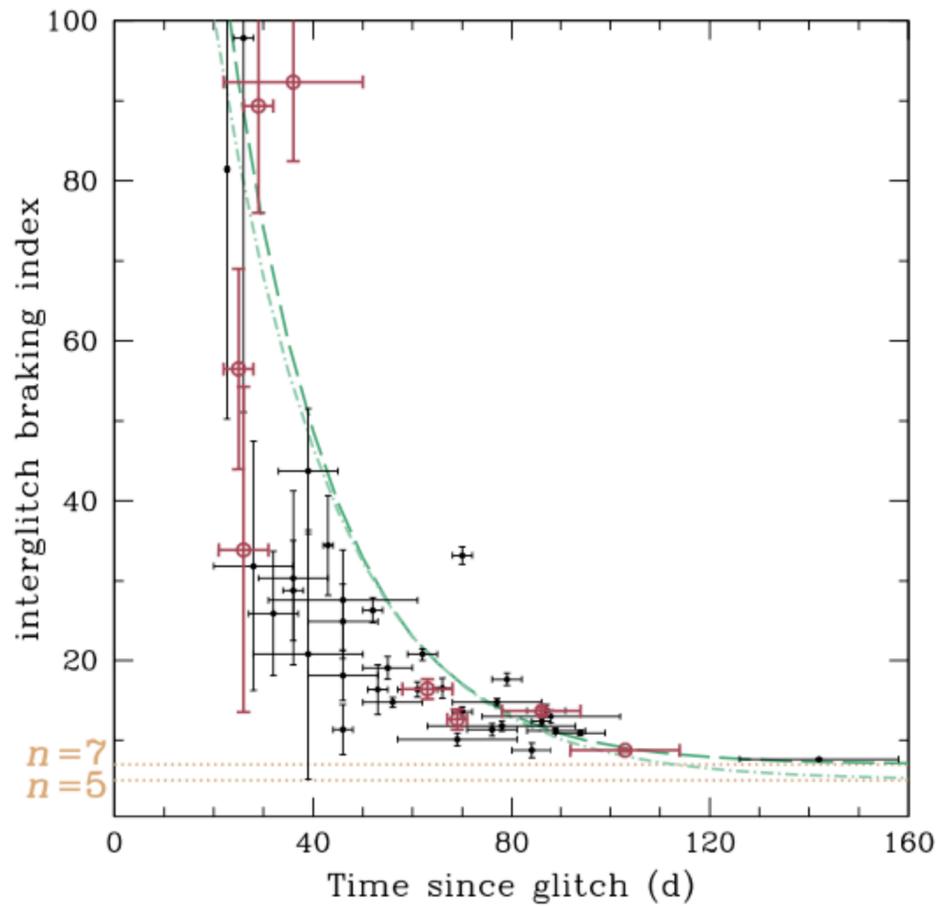
no mountains in its equator, mountain (ellipticity) $< 10^{-8}$
 spin-down of J0711-6830 can not be explained only with GW

Pulsar J0537-6910

arXiv:2012.12926

X-ray Pulsar PSR J0537-6910 @ 160k lyr

= known as the best energy emitter (the maximum spin-down brightness) and also has frequent glitches



Braking index

n=5 (GW from asymmetry of NS)

n=7 (GW via Surface Wave)

no GW detection

no mountains in its equator, mountain < several 10 cm

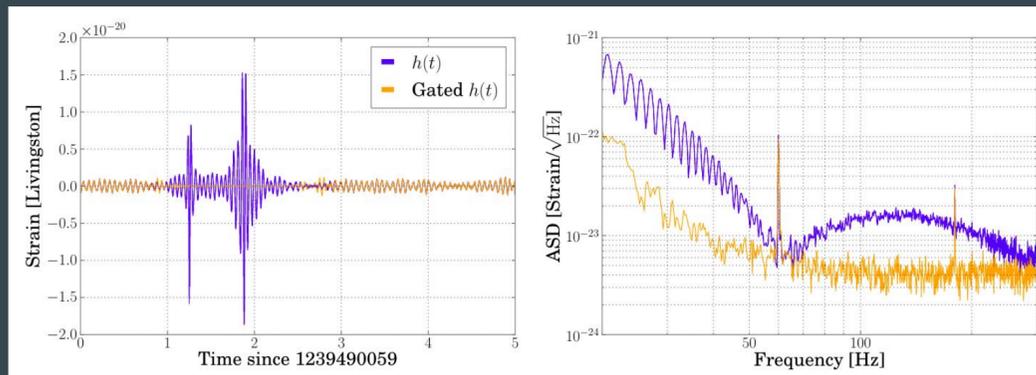
GW emission is less than 14 % of spin-down energy

Upper limits on Isotropic GW background

[arXiv:2101.12130](https://arxiv.org/abs/2101.12130)

Gating

Large population of **loud glitches** in LIGO-H and LIGO-L leads to **removal of >50%** of coincident **lifetime due to non-stationary cut**. Gating **zeroes out** these **glitches** with only introducing a **deadtime of < 1%**. Gating has **no impact** on our ability to **recover a GWB**.



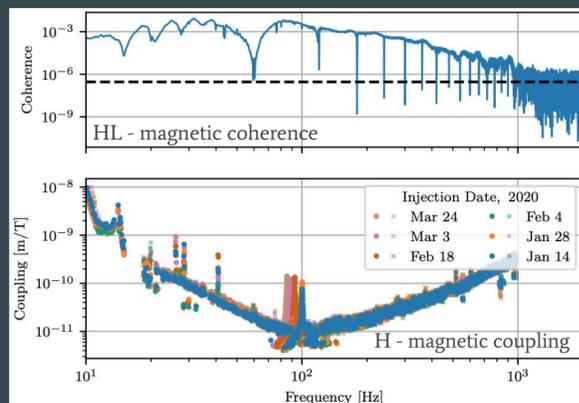
Source: A. Matas, et al. (2020) - [LIGO-P2000546-v2](https://arxiv.org/abs/2005.0546v2)

11

data quality improvement by “Gating” technique

Magnetic noise budget

Global coherent magnetic fields can **mimic a GWB**. This effect is studied by using **precise measurements of the magnetic fields** at the sites and the **coupling** of magnetic fields **to the interferometers**.

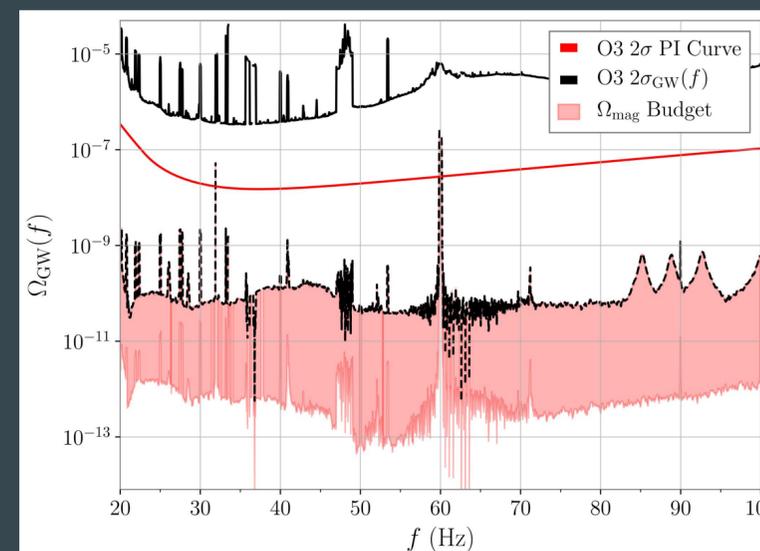


$$\hat{C}_{\text{mag},IJ}(f) = \frac{2}{T} \frac{|T_I(f)||T_J(f)|\text{Re}[\tilde{m}_I^*(f)\tilde{m}_J(f)]}{\gamma_{IJ}(f)S_0(f)}$$

Source: D. Davis, et al. (2021) - [arXiv:2101.11673](https://arxiv.org/abs/2101.11673)

14

Magnetic noise budget



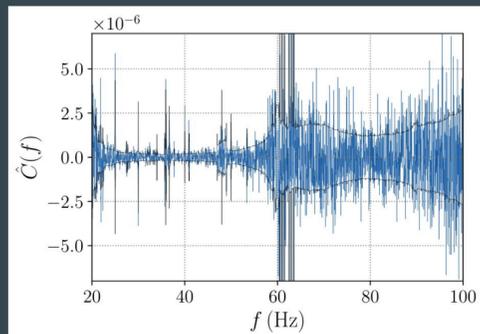
15

Magnetic noise (Schumann resonance) is less than the sensitivity

webinar slide
Feb 5, 2021

Upper limits on Isotropic GW background

Cross-correlation spectra + parameter estimation formalism



- We fit models to O3 data using a hybrid frequentist-Bayesian approach:

$$p(\hat{C}_k^{IJ} | \Theta) \propto \exp \left[-\frac{1}{2} \sum_{IJ} \sum_k \left(\frac{\hat{C}_k^{IJ} - \Omega_M(f_k | \Theta)}{\sigma_{IJ}(f_k)} \right)^2 \right]$$

- Models we consider:
 - Power Law (PL)
 - Scalar-Vector-Tensor PL (SVT-PL)
 - Magnetic (MAG)
 - Compact binary coalescence (CBC)

- H, L and V baselines combined **for the first time!**
- O3 data consistent with uncorrelated, Gaussian noise

16

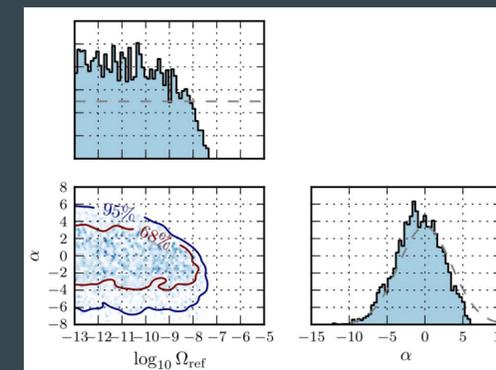
Upper limits (ULs) on PL backgrounds

Two parameters in the PL model:

$$\Omega_{PL}(f) = \Omega_{ref} \left(\frac{f}{f_{ref}} \right)^\alpha$$

We place ULs on Ω_{ref} for different priors:

	Log-uniform prior		
α	O3	O2	Improvement
0	5.8×10^{-9}	3.5×10^{-8}	6.0
2/3	3.4×10^{-9}	3.0×10^{-8}	8.8



17

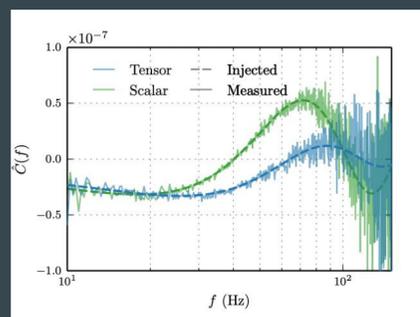
O1+O2+O3 data
(O3 with Virgo)

no GWB detection

Upper limits non-GR backgrounds

$$\Omega_{SVT-PL}(f) = \sum_p \beta_{IJ}^{(p)}(f) \Omega_{ref}^{(p)} \left(\frac{f}{f_{ref}} \right)^{\alpha_p}$$

$$\beta_{IJ}^{(p)}(f) = \gamma_{IJ}^{(p)}(f) / \gamma_{IJ}(f)$$



Callister et al, Phys. Rev. X 7, 041058

For a log-uniform prior on all Ω_{ref} and a marginalized prior on all α ,

Polarization	O3	O2	Improvement
Tensor	6.4×10^{-9}	3.2×10^{-8}	5.0
Vector	7.9×10^{-9}	2.9×10^{-8}	3.7
Scalar	2.1×10^{-8}	6.1×10^{-8}	2.9

18

▲ upper limits on scalar, vector modes

▲ upper limits on Power-Law models

Joint Magnetic + GWB fit

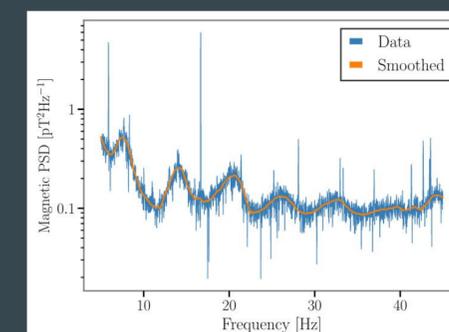
- A *novel approach*, complementary to the magnetic noise budget
- We model the background from the local magnetic field
- We model its coupling to the strain channel of the detectors, the transfer function

$$|T_I(f)| = \kappa_I \left(\frac{f}{10 \text{ Hz}} \right)^{-\beta_I}$$

- Gaussian noise preferred over correlated magnetic noise:
- Gaussian noise preferred over correlated magnetic noise + power law GWB:

$$\log_{10} \mathcal{B}_N^{\text{MAG}} = -0.03$$

$$\log_{10} \mathcal{B}_N^{\text{MAG+PL}} = -0.3$$



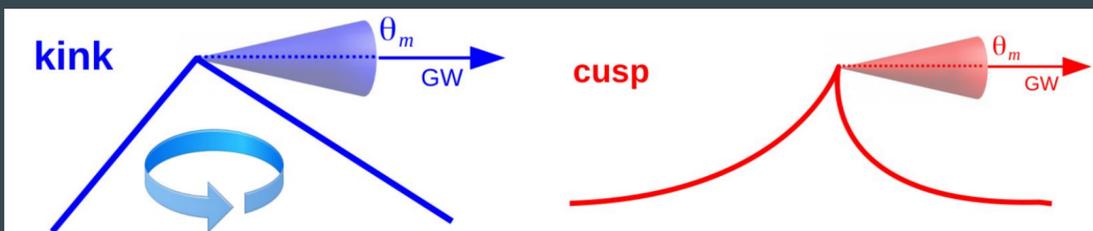
Meyers et al, Phys. Rev. D 102, 102005

19

webinar slide
Feb 5, 2021

Constraints on Cosmic Strings

Cosmic strings: overview and burst search



$$h_i(\ell, z, f) = A_i(\ell, z) f^{-q_i}$$

- Cusps: $q = 4/3$
- Kinks: $q = 5/3$
- **Kink-kink collisions: $q = 2$ (new)**

$$A_i(\ell, z) = g_{1,i} \frac{G\mu \ell^{2-q_i}}{(1+z)^{q_i-1} r(z)}$$

String tension $G\mu$

The number of kinks per loop oscillation has been promoted to a free parameter

Damour and Vilenkin, PhysRevD.64.064008

28

Cosmic strings: overview and burst search

Three different (sets of) models for the population of cosmic string loops

- Model A: Blanco-Pillado et al., PhysRevD.89.023512
- Model B: Lorenz et al., JCAP 10 (2010) 003
- Model(s) C: new set of models that extends both models A and B Auclair et al., JCAP 06 (2019) 015

$$\frac{dR_i}{d\ell dV} = \frac{2}{\ell} N_i \times n(\ell, t) \times \Delta_i \times (1+z)^{-1}$$

$$R = \int dA \varepsilon(A) \frac{dR}{dA}(A, G\mu, N_k)$$

Bursts are assumed to follow Poissonian statistics

$$P(X = k) = \frac{\lambda^k}{k!} e^{-\lambda}, \quad \lambda = T_{\text{obs}} \mathcal{R}$$

Parameters that are not consistent with the non-detection of bursts are excluded

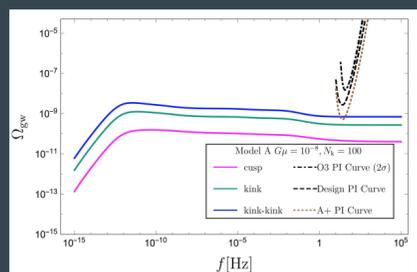
$$P(X = 0) = e^{-T_{\text{obs}} \mathcal{R}} < 5\%$$

$$\mathcal{R} > 2.996 / T_{\text{obs}}$$

webinar slide
Feb 5, 2021

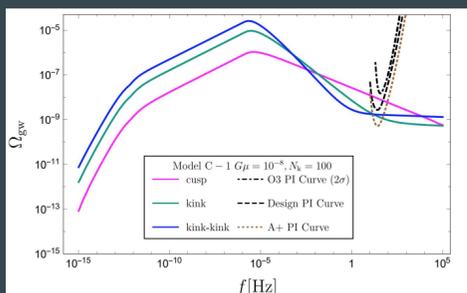
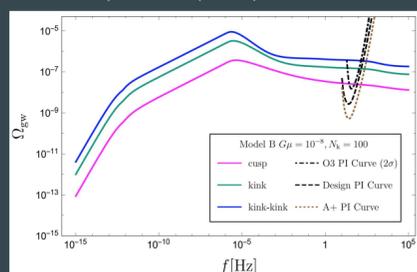
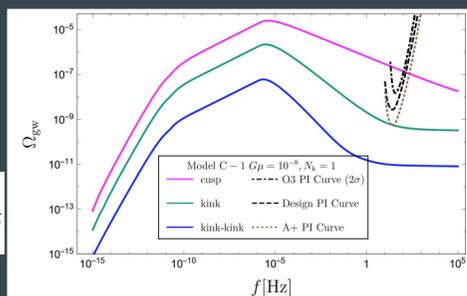
30

Cosmic strings: stochastic search



$$\Omega_{\text{GW}}(f) = \frac{f}{\rho_c} \frac{d\rho_{\text{GW}}}{df}$$

$$\Omega_{\text{GW}}(f) = \frac{4\pi^2}{3H_0^2} f^3 \sum_i \int dz \int d\ell h_i^2 \times \frac{d^2 R_i}{dz d\ell}$$



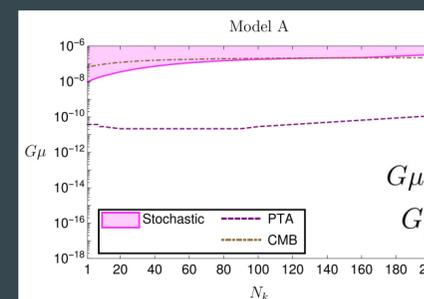
Model A: Blanco-Pillado, Olum, Shlaer, PRD 89, 023512(2014)

Model B: Lorenz, Ringeval, Sakellariadou, JCAP 1010, 003 (2010)

Model C: Auclair, Ringeval, Sakellariadou, Steer, JCAP 06, 015 (2019)

32

Cosmic strings: exclusion plots

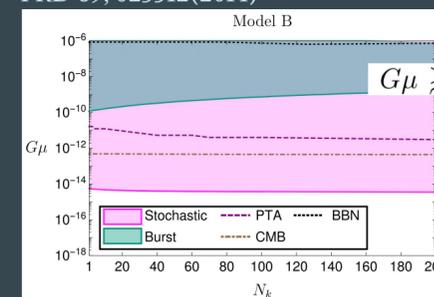


$$G\mu \gtrsim (9.6 \times 10^{-9} - 10^{-6})$$

$$G\mu \gtrsim 10^{-10} \text{ PTA}$$

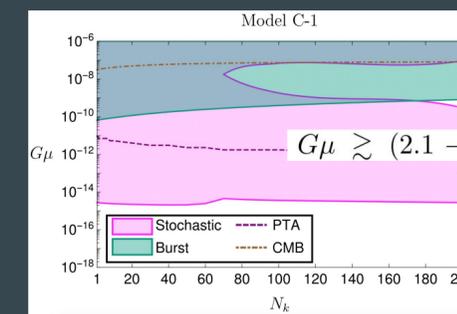
$$N_c = 1$$

Model A: Blanco-Pillado, Olum, Shlaer, PRD 89, 023512(2014)

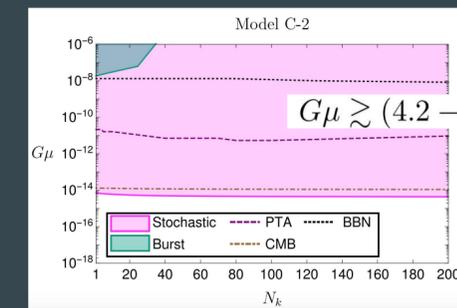


$$G\mu \gtrsim (4.0 - 6.3) \times 10^{-15}$$

Model B: Lorenz, Ringeval, Sakellariadou, JCAP 1010, 003 (2010)



$$G\mu \gtrsim (2.1 - 4.5) \times 10^{-15}$$

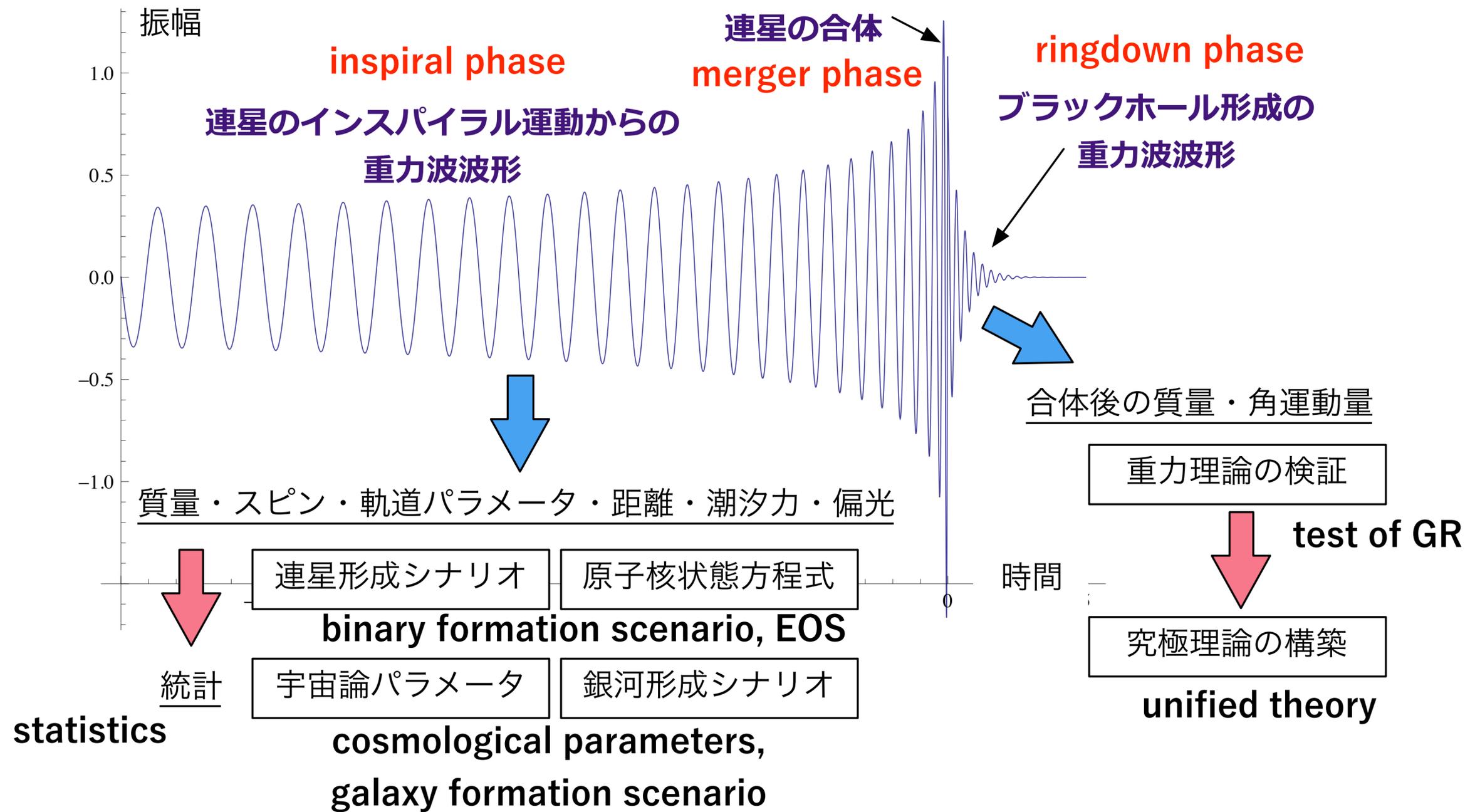


$$G\mu \gtrsim (4.2 - 7.0) \times 10^{-15}$$

Model C: Auclair, Ringeval, Sakellariadou, Steer, JCAP 06, 015 (2019)

34

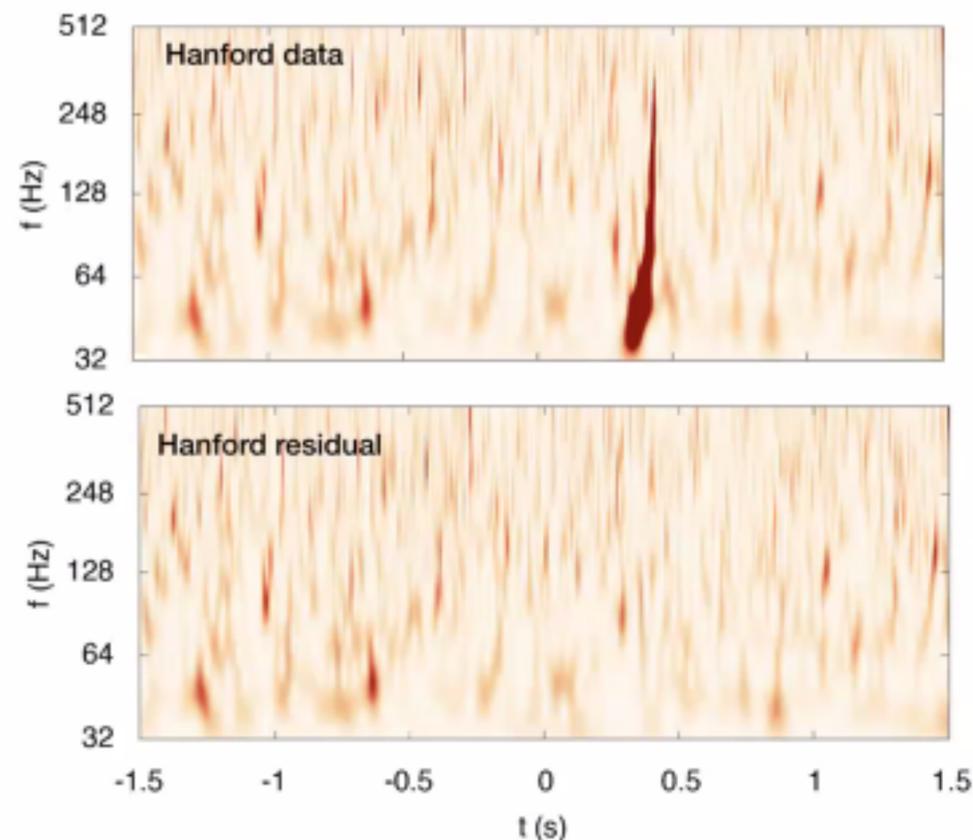
Test of Gravity Theories



GWTC-2: Test of General Relativity by LIGO-Virgo

[arXiv:2010.14529](https://arxiv.org/abs/2010.14529)

1. Residuals test



Subtract the best fit template for the event from the strain data and compute the 90% upper limit on residual SNR.

Check whether the residual SNR is consistent with SNR from noise: measure SNR from noise-only times around the event times, yielding a p -value

$$p = P(\text{SNR}_{\text{noise}}^{90\%} \geq \text{SNR}_{\text{residual}}^{90\%} \mid \text{noise})$$

TABLE III. Results of the residuals analysis (Sec. IV A). For each event, we present the SNR of the subtracted GR waveform (SNR_{GR}), the 90%-credible upper limit on the residual network SNR (SNR_{90}), a corresponding lower limit on the fitting factor (FF_{90}), and the p -value.

Events	SNR_{GR}	Residual SNR_{90}	FF_{90}	p -value
GW190408_181802	16.06	8.48	0.88	0.15
GW190412	18.23	6.67	0.94	0.30
GW190421_213856	10.47	7.52	0.81	0.07
GW190503_185404	13.21	5.78	0.92	0.83
GW190512_180714	12.81	5.92	0.91	0.44
GW190513_205428	12.85	6.44	0.89	0.70
GW190517_055101	11.52	6.40	0.87	0.69
GW190519_153544	15.34	6.38	0.92	0.65
GW190521	14.23	6.34	0.91	0.28
GW190521_074359	25.71	6.15	0.97	0.35
GW190602_175927	13.22	5.46	0.92	0.86
GW190630_185205	16.13	5.13	0.95	0.52
GW190706_222641	13.39	7.80	0.86	0.18
GW190707_093326	13.55	5.89	0.92	0.25
GW190708_232457	13.97	6.00	0.92	0.19
GW190720_000836	10.56	7.30	0.82	0.18
GW190727_060333	11.62	4.88	0.92	0.97
GW190728_064510	13.47	5.98	0.91	0.53
GW190814	25.06	6.43	0.97	0.84
GW190828_063405	16.13	8.47	0.89	0.12
GW190828_065509	9.67	6.30	0.84	0.41
GW190910_112807	14.32	5.60	0.93	0.65
GW190915_235702	13.82	8.30	0.86	0.09
GW190924_021846	12.21	5.91	0.90	0.57

All p -values consistent with residual SNR produced by noise

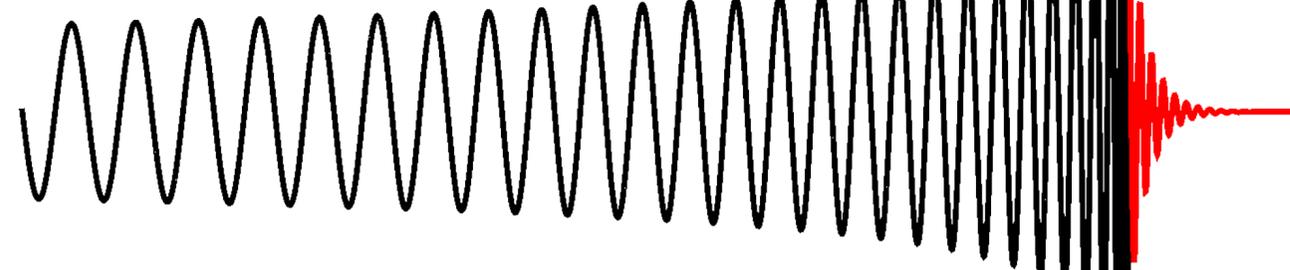
No statistically significant deviations from GR

GWTC-2: Test of General Relativity by LIGO-Virgo

[arXiv:2010.14529](https://arxiv.org/abs/2010.14529)

1. Residuals test

2. Inspiral-merger-ringdown consistency test

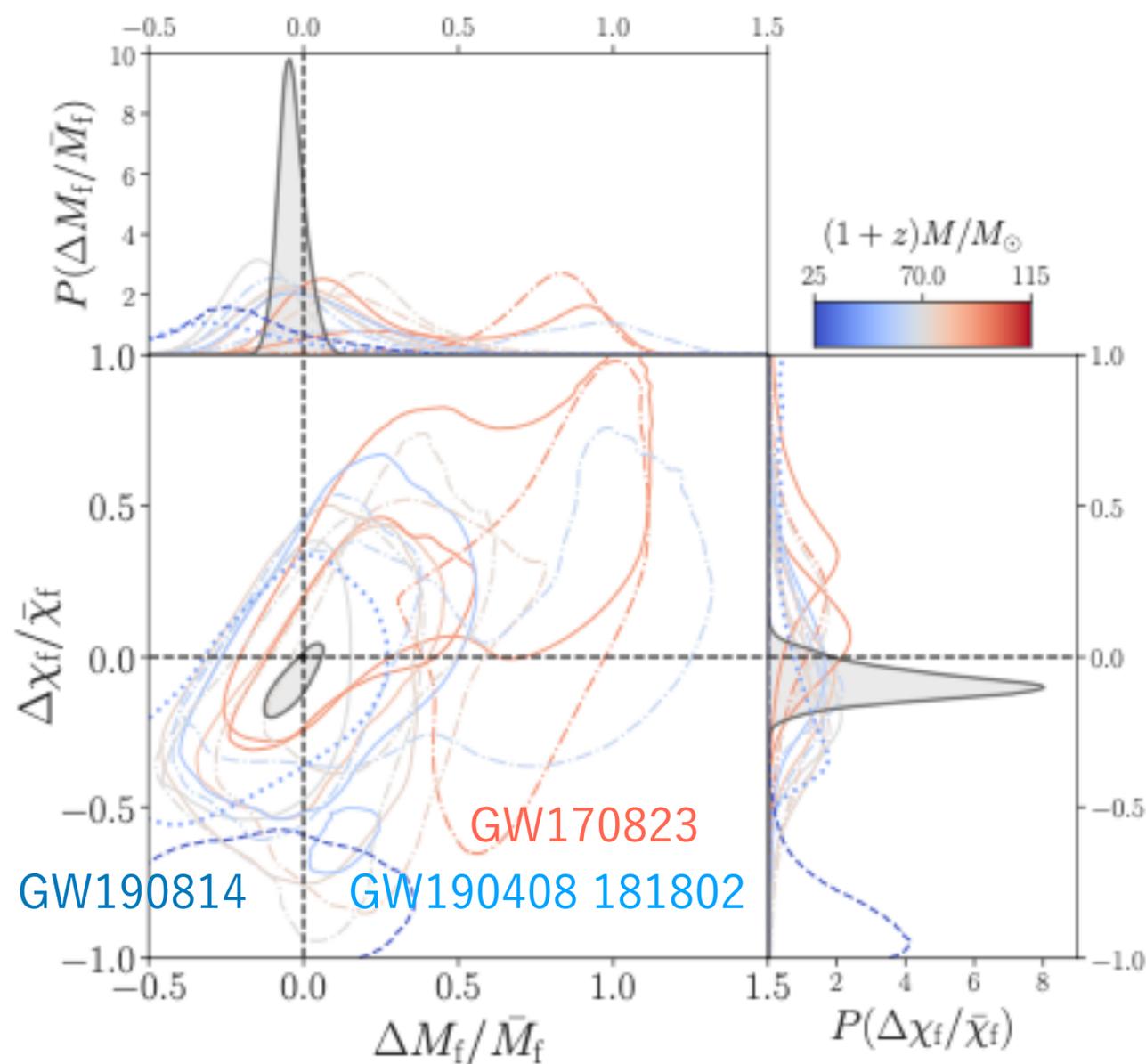


Parameter Estimation with $f < f_c$,

with $f > f_c$,

$$M_f^{\text{insp}}, \chi_f^{\text{insp}}$$

$$M_f^{\text{postinsp}}, \chi_f^{\text{postinsp}}$$



Waveform models

IMRPhenom - phenomenological PN-based models, calibrated to NR

SEOBNR - aligned-spin effective-one-body models, calibrated to NR

(note: only includes quadrupole)

◀ IMRPhenom waveform test mostly consistent, but ...

GW170823 ◀ 39.5M+29.5M, SNR@ inspiral < 8

GW190408 181802 ◀ 24.5M+18.3M, with multimodal posterior

GW190814 ◀ 23M+2.6M, large mass ratio ever

No statistically significant deviations from GR

GWTC-2: Test of General Relativity by LIGO-Virgo

[arXiv:2010.14529](https://arxiv.org/abs/2010.14529)

1. Residuals test
2. IMR consistency test
3. Hierarchical analysis
4. Parametrized test

$$\tilde{h}(f) = A(f) e^{i\varphi(f)}$$

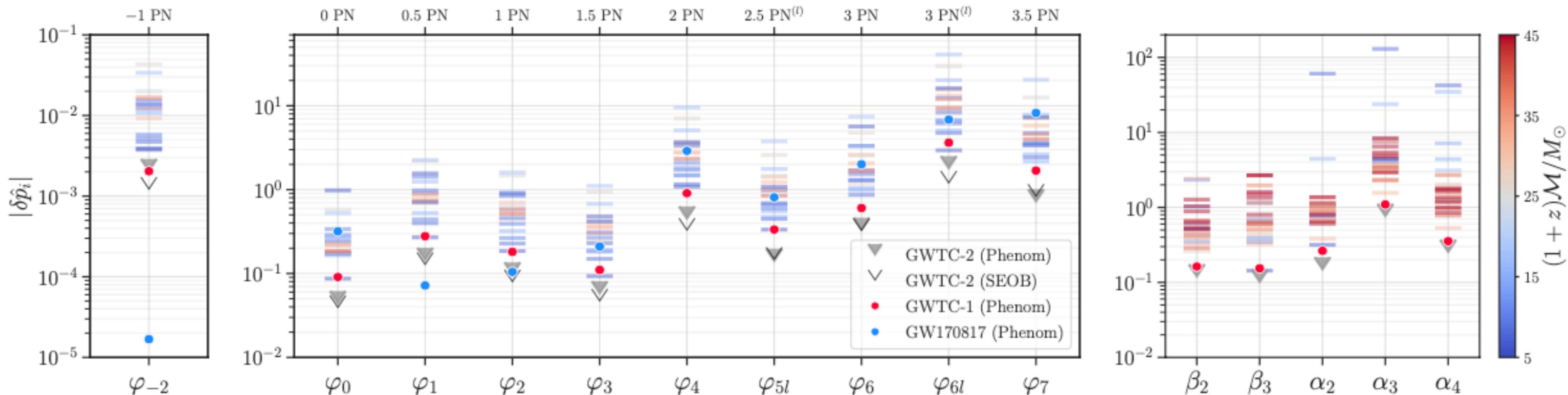
$$\varphi_{\text{inspiral}}(f) = \varphi_{\text{ref}} + 2\pi f t_{\text{ref}} + \varphi_{\text{Newton}}(Mf)^{-5/3} + \varphi_{0.5\text{PN}}(Mf)^{-4/3} + \varphi_{1\text{PN}}(Mf)^{-1} + \varphi_{1.5\text{PN}}(Mf)^{-2/3} + \dots$$

$$\{\delta\varphi_{-2}, \delta\varphi_0, \delta\varphi_1, \dots, \delta\varphi_7\} \propto f^{(i-5)/3}$$

$$\varphi_{\text{intermediate}}(f) = \eta^{-1} \left(\beta_0 + \beta_1 f + \beta_2 \log f - \frac{\beta_3}{3} f^{-3} \right)$$

$$\varphi_{\text{MR}}(f) = \eta^{-1} \left\{ \alpha_0 + \alpha_1 f - \alpha_2 f^{-1} + \frac{4}{3} \alpha_3 f^{3/4} + \alpha_4 \tan^{-1} \left(\frac{f - \alpha_5 f_{\text{RD}}}{f_{\text{damp}}} \right) \right\}$$

$$\eta = m_1 m_2 / M^2$$



No statistically significant deviations from GR

GWTC-2: Test of General Relativity by LIGO-Virgo

arXiv:2010.14529

1. Residuals test
2. IMR consistency test
3. Hierarchical analysis
4. Parametrized test
5. Spin-induced quadrupol
6. Ringdown
7. Echoes
8. Dispersion
9. Polarizations

$$h_+(t) - ih_\times(t) = \sum_{\ell=2}^{+\infty} \sum_{m=-\ell}^{\ell} \sum_{n=0}^{+\infty} \mathcal{A}_{\ell mn} \exp\left[-\frac{t-t_0}{(1+z)\tau_{\ell mn}}\right] \exp\left[\frac{2\pi i f_{\ell mn}(t-t_0)}{1+z}\right] {}_{-2}S_{\ell mn}(\theta, \phi, \chi_f)$$

Event	Redshifted final mass (1+z)M _f [M _⊙]				Final spin χ _f				Higher modes	Overtones	
	IMR	Kerr ₂₂₀	Kerr ₂₂₁	Kerr _{HM}	IMR	Kerr ₂₂₀	Kerr ₂₂₁	Kerr _{HM}	log ₁₀ B ₂₂₀ ^{HM}	log ₁₀ B ₂₂₀ ²²¹	log ₁₀ O _{GR} ^{modGR}
GW150914	68.8 ^{+3.6} _{-3.1}	62.7 ^{+19.0} _{-12.1}	71.7 ^{+13.2} _{-12.5}	80.3 ^{+20.1} _{-21.7}	0.69 ^{+0.05} _{-0.04}	0.52 ^{+0.33} _{-0.44}	0.69 ^{+0.18} _{-0.36}	0.83 ^{+0.13} _{-0.45}	0.03	0.63	-0.34
GW170104	58.5 ^{+4.6} _{-4.1}	56.2 ^{+19.1} _{-11.6}	61.3 ^{+16.7} _{-13.2}	104.3 ^{+207.7} _{-43.1}	0.66 ^{+0.08} _{-0.11}	0.26 ^{+0.42} _{-0.24}	0.51 ^{+0.34} _{-0.44}	0.59 ^{+0.34} _{-0.51}	0.26	-0.20	-0.23
GW170814	59.7 ^{+3.0} _{-2.3}	46.1 ^{+133.0} _{-33.6}	56.6 ^{+20.9} _{-11.1}	171.2 ^{+268.7} _{-143.5}	0.72 ^{+0.07} _{-0.05}	0.52 ^{+0.42} _{-0.47}	0.47 ^{+0.40} _{-0.42}	0.54 ^{+0.41} _{-0.48}	0.04	-0.19	-0.11
GW170823	88.8 ^{+11.2} _{-10.2}	73.8 ^{+26.8} _{-23.7}	79.0 ^{+21.3} _{-13.2}	103.0 ^{+133.1} _{-46.7}	0.72 ^{+0.09} _{-0.12}	0.46 ^{+0.40} _{-0.41}	0.36 ^{+0.38} _{-0.32}	0.74 ^{+0.22} _{-0.61}	0.02	-0.98	-0.07
GW190408_181802	53.1 ^{+3.2} _{-3.4}	22.4 ^{+253.0} _{-11.1}	46.6 ^{+18.8} _{-10.9}	127.4 ^{+327.7} _{-107.6}	0.67 ^{+0.06} _{-0.07}	0.45 ^{+0.45} _{-0.40}	0.36 ^{+0.46} _{-0.33}	0.46 ^{+0.47} _{-0.41}	-0.05	-1.02	-0.02
GW190512_180714	43.4 ^{+4.1} _{-2.8}	37.6 ^{+48.9} _{-22.4}	36.7 ^{+19.3} _{-24.8}	99.4 ^{+247.6} _{-66.5}	0.65 ^{+0.07} _{-0.07}	0.41 ^{+0.47} _{-0.37}	0.45 ^{+0.40} _{-0.39}	0.77 ^{+0.20} _{-0.66}	0.09	-0.42	0.03
GW190513_205428	70.8 ^{+12.2} _{-6.9}	55.5 ^{+31.5} _{-42.1}	68.5 ^{+28.2} _{-11.8}	88.7 ^{+250.0} _{-41.9}	0.69 ^{+0.14} _{-0.12}	0.38 ^{+0.48} _{-0.34}	0.31 ^{+0.53} _{-0.28}	0.59 ^{+0.34} _{-0.52}	0.09	-0.54	-0.05
GW190519_153544	148.2 ^{+14.5} _{-15.5}	120.7 ^{+39.7} _{-21.5}	125.9 ^{+24.3} _{-21.7}	155.4 ^{+84.4} _{-42.5}	0.80 ^{+0.07} _{-0.12}	0.42 ^{+0.41} _{-0.36}	0.52 ^{+0.25} _{-0.40}	0.70 ^{+0.21} _{-0.50}	0.21	-0.00	-0.11
GW190521	259.2 ^{+36.6} _{-29.0}	282.2 ^{+50.0} _{-61.9}	284.0 ^{+40.4} _{-43.9}	299.3 ^{+57.7} _{-62.4}	0.73 ^{+0.11} _{-0.14}	0.76 ^{+0.14} _{-0.38}	0.78 ^{+0.10} _{-0.22}	0.80 ^{+0.13} _{-0.30}	0.12	-0.86	-0.50
GW190521_074359	88.1 ^{+4.3} _{-4.9}	83.0 ^{+24.0} _{-17.2}	86.4 ^{+14.1} _{-14.8}	105.9 ^{+20.8} _{-26.4}	0.72 ^{+0.05} _{-0.07}	0.57 ^{+0.31} _{-0.49}	0.67 ^{+0.17} _{-0.34}	0.87 ^{+0.09} _{-0.39}	-0.04	1.29	-0.27
GW190602_175927	165.6 ^{+20.5} _{-19.2}	156.4 ^{+71.4} _{-30.6}	160.0 ^{+37.4} _{-31.2}	261.7 ^{+84.4} _{-91.5}	0.71 ^{+0.10} _{-0.13}	0.34 ^{+0.41} _{-0.31}	0.46 ^{+0.31} _{-0.39}	0.79 ^{+0.14} _{-0.49}	0.61	-1.56	0.32
GW190706_222641	173.6 ^{+18.8} _{-22.9}	136.0 ^{+52.0} _{-29.3}	152.5 ^{+37.8} _{-28.4}	184.0 ^{+139.2} _{-55.8}	0.80 ^{+0.08} _{-0.17}	0.41 ^{+0.42} _{-0.37}	0.55 ^{+0.31} _{-0.45}	0.68 ^{+0.26} _{-0.54}	-0.06	-0.64	-0.45
GW190708_232457	34.4 ^{+2.7} _{-0.7}	28.9 ^{+285.4} _{-17.9}	32.3 ^{+15.0} _{-12.2}	171.9 ^{+307.6} _{-147.8}	0.69 ^{+0.04} _{-0.04}	0.47 ^{+0.45} _{-0.42}	0.34 ^{+0.44} _{-0.31}	0.43 ^{+0.51} _{-0.39}	-0.11	-0.17	-0.02
GW190727_060333	100.0 ^{+10.5} _{-10.0}	78.7 ^{+45.7} _{-66.4}	88.8 ^{+25.7} _{-16.0}	107.4 ^{+112.1} _{-42.7}	0.73 ^{+0.10} _{-0.10}	0.53 ^{+0.42} _{-0.47}	0.45 ^{+0.39} _{-0.41}	0.71 ^{+0.24} _{-0.59}	-0.02	-1.65	-0.40
GW190828_063405	75.9 ^{+6.0} _{-5.2}	71.2 ^{+35.8} _{-55.5}	69.6 ^{+22.0} _{-17.3}	99.0 ^{+166.0} _{-49.1}	0.76 ^{+0.06} _{-0.07}	0.72 ^{+0.25} _{-0.62}	0.65 ^{+0.27} _{-0.55}	0.92 ^{+0.06} _{-0.74}	0.05	-0.72	-0.05
GW190910_112807	97.3 ^{+9.4} _{-7.1}	112.2 ^{+32.0} _{-31.7}	107.7 ^{+28.6} _{-27.4}	137.1 ^{+59.5} _{-31.4}	0.70 ^{+0.08} _{-0.07}	0.76 ^{+0.18} _{-0.55}	0.75 ^{+0.17} _{-0.46}	0.91 ^{+0.07} _{-0.27}	-0.10	-0.64	-0.40
GW190915_235702	75.0 ^{+7.7} _{-7.3}	38.3 ^{+335.1} _{-27.4}	63.0 ^{+19.1} _{-9.9}	137.3 ^{+324.1} _{-96.2}	0.71 ^{+0.09} _{-0.11}	0.52 ^{+0.43} _{-0.46}	0.27 ^{+0.40} _{-0.24}	0.55 ^{+0.39} _{-0.49}	0.06	-0.37	-0.04

No significant evidence for higher-mode in ringdown part

Statistical Approaches

* BH Spectroscopy with coherent mode stacking

PRL **118**, 161101 (2017) PHYSICAL REVIEW LETTERS week ending
21 APRIL 2017

Black Hole Spectroscopy with Coherent Mode Stacking

Huan Yang,¹ Kent Yagi,¹ Jonathan Blackman,² Luis Lehner,^{3,4} Vasileios Paschalidis,¹ Frans Pretorius,^{1,4} and Nicolás Yunes⁵

¹*Department of Physics, Princeton University, Princeton, New Jersey 08544, USA*
²*TAPIR, Walter Burke Institute for Theoretical Physics, California Institute of Technology, Pasadena, California 91125, USA*
³*Perimeter Institute for Theoretical Physics, Waterloo, Ontario N2L 2Y5, Canada*
⁴*CIFAR, Cosmology and Gravity Program, Toronto, Ontario M5G 1Z8, Canada*
⁵*eXtreme Gravity Institute, Department of Physics, Montana State University, Bozeman, Montana 59717, USA*

(Received 20 January 2017; published 20 April 2017)

* Hierarchical Test

PHYSICAL REVIEW LETTERS **123**, 121101 (2019)

Hierarchical Test of General Relativity with Gravitational Waves

Maximiliano Isi^{1,2,*}, Katerina Chatziioannou,^{1,†} and Will M. Farr^{1,3,‡}

¹*Center for Computational Astrophysics, Flatiron Institute, 162 5th Ave, New York, New York 10010, USA*
²*LIGO Laboratory and Kavli Institute for Astrophysics and Space Research, Massachusetts Institute of Technology, Cambridge, Massachusetts 02139, USA*
³*Department of Physics and Astronomy, Stony Brook University, Stony Brook, New York 11794, USA*

 (Received 5 May 2019; published 16 September 2019)

* “parametrized ringdown spin expansion coefficients” (ParSpec)

PHYSICAL REVIEW D **101**, 024043 (2020)

Parametrized ringdown spin expansion coefficients: A data-analysis framework for black-hole spectroscopy with multiple events

Andrea Maselli¹, Paolo Pani¹, Leonardo Gualtieri,¹ and Emanuele Berti²

¹*Dipartimento di Fisica, “Sapienza” Università di Roma, Piazzale Aldo Moro 5, 00185, Roma, Italy*
²*Department of Physics and Astronomy, John Hopkins University, Baltimore, Maryland 21218, USA*

 (Received 31 October 2019; published 22 January 2020)

BH Spectroscopy with coherent mode stacking

SNR of GW150914 ringdown ~ 7

higher modes can be seen SNR ~ 45

* Ringdown part = (2,2) + (3,3) modes

$$s_j = n_j + h_{22,j} + h_{33,j}, \quad h_{\ell m,j}(t) = A_{\ell m,j} e^{-\gamma_{\ell m,j} t} \sin(\omega_{\ell m,j} t - \phi_{\ell m,j})$$

* Pick up one event (ith) as the base case.

Rescale (3,3) freq. equal to all events.

secondary mode phase offset $\tilde{\phi}_{33,i} \equiv \phi_{33}$ and frequency $\tilde{\omega}_{33,i} \equiv \omega_{33}$. Specifically, we scale and shift each signal in time via $\tilde{s}_j(t) \equiv s_j(t/\alpha_j + \Delta_j)$, with $\alpha_j \equiv \omega_{33,j}/\omega_{33}$ and $\Delta_j \equiv (\phi_{33,j} - \phi_{33})/\omega_{33,j}$.

* Sum up all events in freq mode

$$\tilde{s}_j(f) \equiv \alpha_j e^{i\omega_{33}\Delta_j} \tilde{s}_j(\alpha_j f), \quad \tilde{\mathbf{s}} = \sum_j c_j \tilde{\mathbf{s}}_j \equiv \tilde{\mathbf{n}} + \tilde{\mathbf{h}}_{22} + \tilde{\mathbf{h}}_{33}$$

$$h_{22} \in (0.623, 2/3)\omega_{33} \text{ for } a=[0,1]$$

* inspiral+merger+ringdown (IMR) waveform models in GR

▶ (M, spin) can be fixed

▶ QNM, phase offsets, amplitudes for all modes in GR can be computed

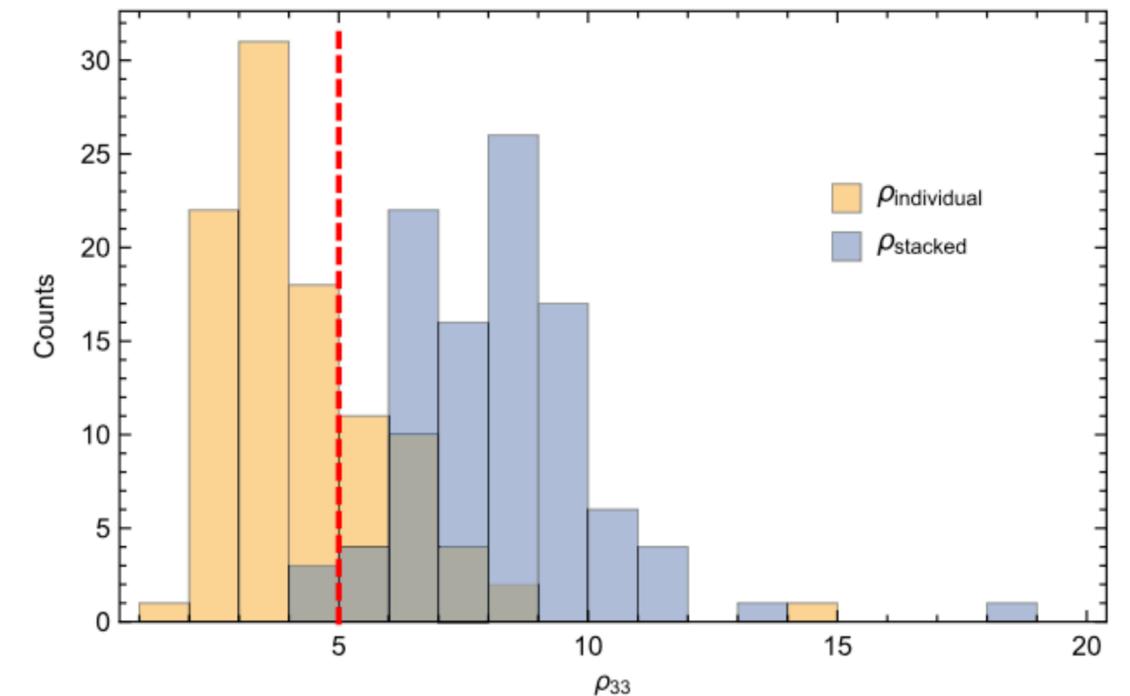
PRL 118, 161101 (2017) PHYSICAL REVIEW LETTERS week ending 21 APRIL 2017

Black Hole Spectroscopy with Coherent Mode Stacking

Huan Yang,¹ Kent Yagi,¹ Jonathan Blackman,² Luis Lehner,^{3,4} Vasileios Paschalidis,¹ Frans Pretorius,^{1,4} and Nicolás Yunes⁵

¹Department of Physics, Princeton University, Princeton, New Jersey 08544, USA
²TAPIR, Walter Burke Institute for Theoretical Physics, California Institute of Technology, Pasadena, California 91125, USA
³Perimeter Institute for Theoretical Physics, Waterloo, Ontario N2L 2Y5, Canada
⁴CIFAR, Cosmology and Gravity Program, Toronto, Ontario M5G 1Z8, Canada
⁵eXtreme Gravity Institute, Department of Physics, Montana State University, Bozeman, Montana 59717, USA

(Received 20 January 2017; published 20 April 2017)



“parametrized ringdown spin expansion coefficients” (ParSpec)

PARSPEC

- Can we find a **consistent framework** to produce **generic constraints** valid for **specific modified theories** of gravity, without losing generality?

- **Perturbatively**: yes. Recently provided by Maselli, Pani, Gualtieri, Berti:

$$\omega_K = \frac{1}{M} \sum_{j=0}^{N_{max}} \chi^j \omega_K^{(j)} (1 + \gamma \delta\omega_K^{(j)})$$

$$\tau_K = M \sum_{j=0}^{N_{max}} \chi^j \tau_K^{(j)} (1 + \gamma \delta\tau_K^{(j)})$$

Proportional to action coupling(s):

$$\gamma := \left(\frac{\ell c^2 (1+z)}{GM} \right)^p$$

Add deviations at each given order.

Also numerical constants!
Independent of specific signal.

11

PRD 101, 024043 (2020)

Gregorio Carullo
<https://dcc.ligo.org/P2000538>



THEORY PARAMETER SPACE

- **p=0** (e.g. certain **scalar-tensor** or **Lorentz-violating**)

$$S_{\mathcal{AE}} = \frac{1}{16\pi G_{\mathcal{AE}}} \int \sqrt{-g} (R - M^{\alpha\beta}{}_{\mu\nu} \nabla_{\alpha} u^{\mu} \nabla_{\beta} u^{\nu}) d^4x$$

- **p=2** (e.g. **Kerr-Newman** or Dark photon)

$$\mathcal{L} = \sqrt{-g} \left(\frac{R}{16\pi} - \frac{1}{4} F_{\mu\nu} F^{\mu\nu} - \frac{1}{4} B_{\mu\nu} B^{\mu\nu} + 4\pi e j_{em}^{\mu} A_{\mu} + 4\pi e_h j_h^{\mu} B_{\mu} + 4\pi \epsilon \epsilon j_h^{\mu} A_{\mu} \right)$$

- **p=4** (e.g. **Einstein-scalar-Gauss-Bonnet** or **dynamical Chern-Simons**)

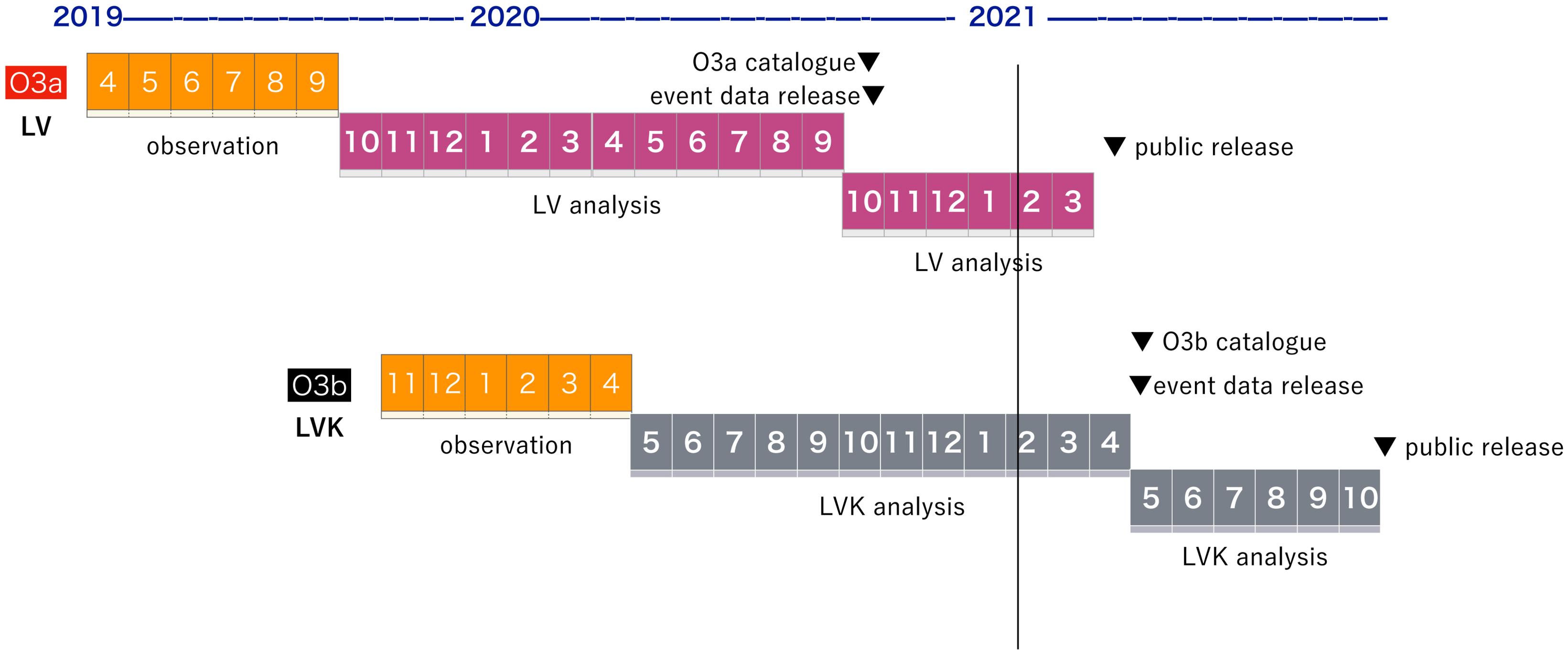
$$S \equiv \int \frac{m_{pl}^2}{2} d^4x \sqrt{-g} \left[R - \frac{1}{2} (\partial\vartheta)^2 + 2\alpha_{GB} f(\vartheta) \mathcal{R}_{GB} \right], \quad S \equiv \int d^4x \sqrt{-g} \left(\frac{m_{pl}^2}{2} R - \frac{1}{2} (\partial\vartheta)^2 - \frac{m_{pl}}{8} \ell^2 \vartheta^* R R \right)$$

- **p=6** (e.g. **Effective Field Theories**)

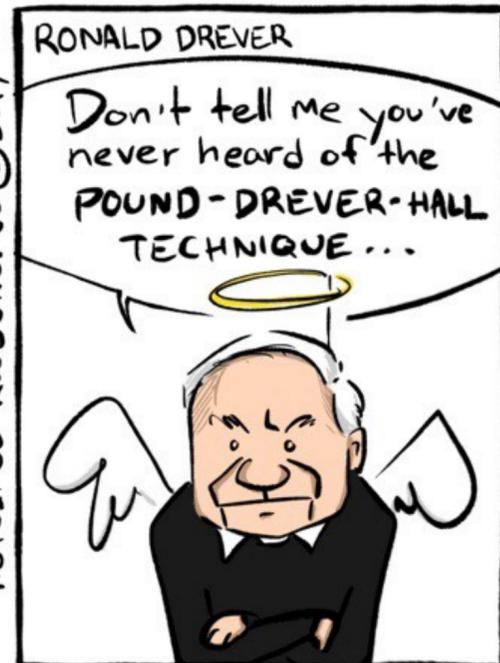
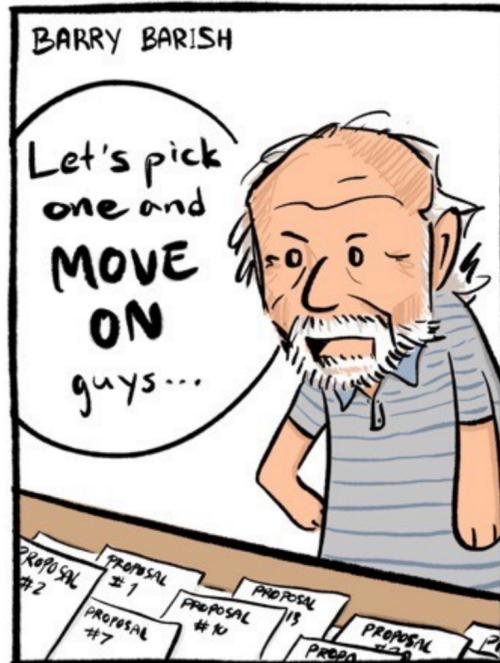
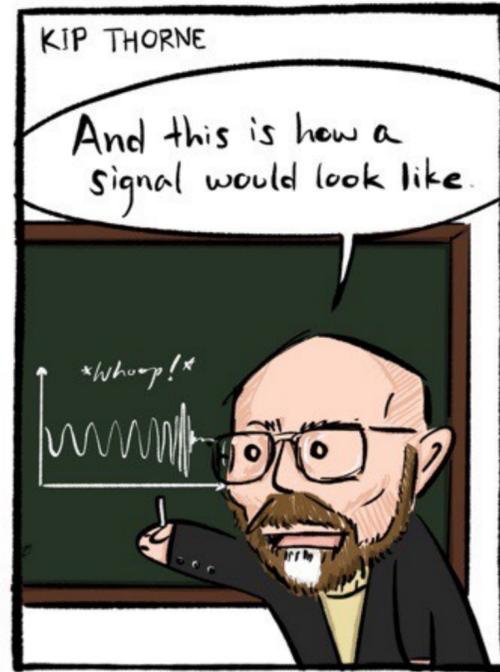
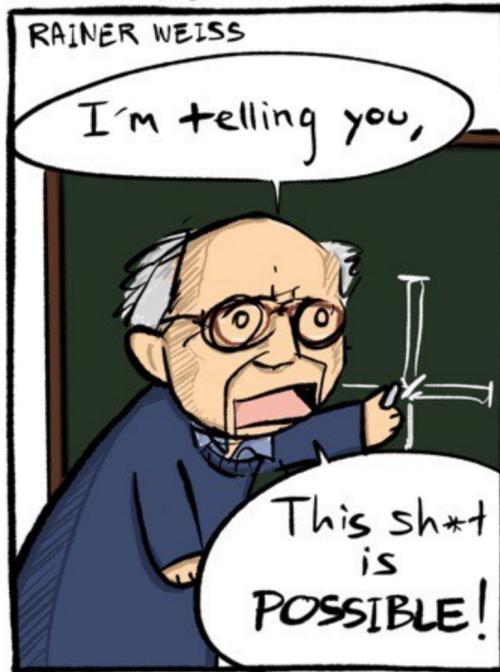
$$S_{\text{eff}} = \int d^4x \sqrt{-g} 2M_{pl}^2 \left(R - \frac{\mathcal{C}^2}{\Lambda^6} - \frac{\tilde{\mathcal{C}}^2}{\tilde{\Lambda}^6} - \frac{\tilde{\mathcal{C}}\mathcal{C}}{\Lambda^6} \right)$$

14

Public Data Release

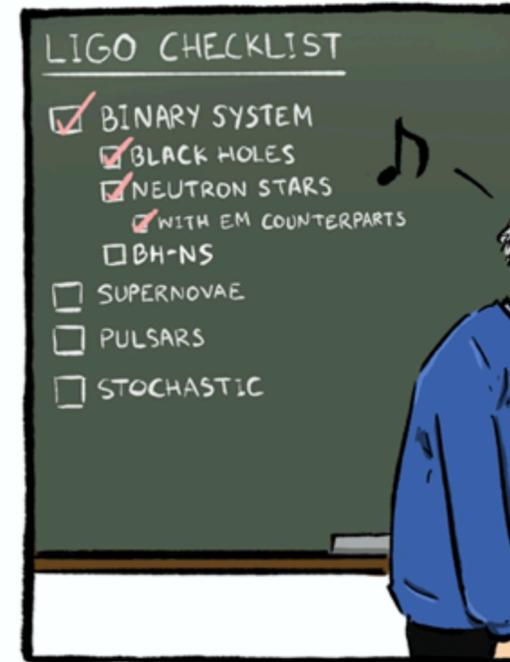


THE NOBEL PRIZE IN PHYSICS 2017



NUTSINEE KIJBUNCHOO © 2017

ANTIMATTERWEBCOMICS.COM



NUTSINEE KIJBUNCHOO © 2017

ANTIMATTERWEBCOMICS.COM

<https://antimatterwebcomics.com/comic/physics-nobel-prize-2017/>

<https://antimatterwebcomics.com/comic/gw170817/>